Monthly Notices
of the
ROYAL ASTRONOMICAL SOCIETY

MNRAS **448,** 732–753 (2015) doi:10.1093/mnras/stu2712

On the environments of Type Ia supernovae within host galaxies

J. P. Anderson,[1⋆] P. A. James,[2] F. Förster,[3,4] S. González-Gaitán,[3,5]
S. M. Habergham,[2] M. Hamuy[3,5] and J. D. Lyman[6]

[1]*European Southern Observatory, Alonso de Cordova 3107, Vitacura, Casilla 19001, Santiago, Chile*
[2]*Astrophysics Research Institute, Liverpool John Moores University, IC2, Liverpool Science Park, 146 Brownlow Hill, Liverpool L3 5RF, UK*
[3]*Millennium Institute of Astrophysics, Santiago, Chile*
[4]*Center for Mathematical Modelling, Universidad de Chile, Avenida Blanco Encalada 2120 Piso 7, Santiago, Chile*
[5]*Departamento de Astronomía, Universidad de Chile, Casilla 36-D, Santiago, Chile*
[6]*Department of Physics, University of Warwick, Coventry CV4 7AL, UK*

Accepted 2014 December 18. Received 2014 December 15; in original form 2014 October 15

ABSTRACT

We present constraints on Type Ia supernovae (SNe Ia) progenitors through an analysis of the environments found at the explosion sites of 102 events within star-forming host galaxies. Hα and *Galaxy Evolution Explorer* near-ultraviolet (UV) images are used to trace on-going and recent star formation (SF), while broad-band *B*, *R*, *J*, *K* imaging is also analysed. Using pixel statistics we find that SNe Ia show the lowest degree of association with Hα emission of all supernova (SN) types. It is also found that they do not trace near-UV emission. As the latter traces SF on time-scales less than 100 Myr, this rules out any extreme 'prompt' delay times as the dominant progenitor channel of SNe Ia. SNe Ia best trace the *B*-band light distribution of their host galaxies. This implies that the population within star-forming galaxies is dominated by relatively young progenitors. Splitting SNe by their $(B - V)$ colours at maximum light, 'redder' events show a higher degree of association with H II regions and are found more centrally within hosts. We discuss possible explanations of this result in terms of line-of-sight extinction and progenitor effects. No evidence for correlations between SN stretch and environment properties is observed.

Key words: supernovae: general – galaxies: statistics.

1 INTRODUCTION

Type Ia supernovae (SNe Ia) are considered to arise from the accretion of matter on to a white dwarf (WD) star in a binary system. This process is thought to increase the WD mass to the point where ignition leads to a runaway thermonuclear explosion of the WD system (see Wang & Han 2012; Maoz, Mannucci & Nelemans 2014 for recent reviews). Indeed, for the very nearby SN Ia, SN 2011fe, the primary progenitor star was directly constrained to be a compact degenerate object for the first time (Nugent et al. 2011; Bloom et al. 2012, also see SN 2013dy, Zheng et al. 2013). However, many processes remain poorly constrained meaning that we still have little idea on the exact explosion physics or the progenitor parameter space that permits a successful explosion. These issues are particularly pertinent given the use of SNe Ia in many areas of astrophysics. SNe Ia have been used as accurate distance indicators, which led to the discovery of the accelerated expansion of the Universe (Riess et al. 1998; Perlmutter et al. 1999). In addition, SNe Ia are the main producers of iron peak elements in the Universe and hence are particularly important for understanding chemical evolution processes (see e.g. Matteucci et al. 2006; Kobayashi & Nomoto 2009, and references therein).

While the exact details of the progenitor systems remain unclear, the two most popular are the single degenerate (SD) and double degenerate (DD) scenarios. In the SD scenario (e.g. Whelan & Iben 1973), a WD accretes matter from a companion main-sequence (MS) or red giant (RG) star, increasing its mass towards the Chandrasekhar mass, which leads to carbon ignition and ensuing explosion. In the DD scenario (e.g. Iben & Tutukov 1984), a double WD system loses angular momentum due to gravitational wave emission, leading to coalescence and explosion. There also exist scenarios where the WD ignites and explodes at masses both below (e.g. Nomoto 1982) and above (e.g. Hachisu et al. 2012; Pakmor et al. 2012 and references therein) the Chandrasekhar mass. Indeed, Scalzo et al. (2014) showed that a significant fraction of 'normal' SNe Ia explode with significantly sub-Chandrasekhar ejecta masses. Various lines of evidence have been presented, much coming in recent years, however a preference for one specific progenitor system for the majority of SNe Ia events is still lacking.

⋆E-mail: janderso@eso.org

The initial classification of SNe into massive stars which core-collapse (CC SNe), and lower mass progenitor systems which lead to thermonuclear explosions was given credence by the observation that CC SNe (SNe II and SNe Ibc) are exclusively observed to occur in star-forming galaxies, while SNe Ia are found to explode in all galaxy types (e.g. van den Bergh, Li & Filippenko 2002). Given that elliptical galaxies are dominated by old stellar populations, this constrains at least a fraction of the progenitors of SNe Ia to be similarly evolved systems. More involved studies have investigated how the SN Ia rate changes with redshift together with host galaxy properties such as colour, mass, star formation rate (SFR), and specific SFR (sSFR) (e.g. Strolger et al. 2004; Mannucci et al. 2005; Förster et al. 2006; Sullivan et al. 2006). These results have been used to constrain the delay time distribution (DTD) of SNe Ia (distribution of times between epoch of star formation, SF, and explosion), with claims of 'prompt' and 'tardy' components (see e.g. Scannapieco & Bildsten 2005; Mannucci, Della Valle & Panagia 2006). Indeed the SN Ia rate is consistent with the 'prompt' component being proportional to the SFR, and the 'tardy' component being consistent with stellar mass of host galaxies (see e.g. Sullivan et al. 2006, and more recently Smith et al. 2012). DTDs have also been derived using the star formation history (SFH) of galaxies within a given SN search program (Maoz et al. 2011; Maoz, Mannucci & Brandt 2012).

The defining characteristic that has allowed SNe Ia to be used as distance indicators is their low intrinsic peak luminosity dispersion (∼0.35 mag; Branch & Miller 1993). This dispersion is lowered further once correlations between luminosities and both SN decline rates and intrinsic colours are adopted (Phillips 1993; Hamuy et al. 1996a; Riess, Press & Kirshner 1996). Investigations have proceeded to find correlations between light-curve parameters and host galaxy properties. Hamuy et al. (2000) (following Hamuy et al. 1996b) found that brighter SNe Ia are preferentially found within younger stellar populations. These initial results have been confirmed (see e.g. Johansson et al. 2013) and further investigated, with indications that brighter events also prefer lower metallicity galaxies (Gallagher et al. 2008; Howell et al. 2009; Neill et al. 2009). These differences would only be important for cosmological studies if correlations remained *after* SN luminosities had been corrected for light-curve properties. Numerous recent studies have concentrated on searching for such correlations with Hubble residuals. Indeed, evidence has now been presented from multiple independent investigators that Hubble residuals show correlations with host galaxy properties, in particular galaxy mass (Kelly et al. 2010; Lampeitl et al. 2010; Sullivan et al. 2010; D'Andrea et al. 2011; Gupta et al. 2011; Childress et al. 2013; Hayden et al. 2013; Johansson et al. 2013; Pan et al. 2014). This could have important consequences for the continued use of SNe Ia as accurate distance indicators out to higher redshifts, if these effects are not properly accounted for. While determining whether stellar population age or metallicity is the driving factor behind these correlations is somewhat difficult, several studies have strongly argued that progenitor age is the dominant parameter, with lower mass, higher sSFR galaxies producing younger SN Ia explosions (Childress et al. 2013; Johansson et al. 2013; Rigault et al. 2013).

While many large samples of global SN Ia host galaxy property studies have now been published, studies of the environments of SNe Ia *within* host galaxies, such as those now regularly seen for CC SNe (see e.g. Modjaz et al. 2008; Anderson et al. 2012; Kelly & Kirshner 2012 and references therein), are to-date rare in the literature. The obvious reason for this is the significantly older progenitor populations of SNe Ia – and the therefore increased delay between SF and explosion – implies that the majority of SNe Ia will explode far from their birth places. This could then restrict the relevance of information that can be extracted from such studies. However, some work in this direction does exist.

The first approach involved investigating the radial distribution of SNe, to see whether different SNe Ia preferentially occur at specific radial positions within galaxies. Given that stellar population properties such as age, extinction, and metallicity change with radial positions, one can associate SN properties to those of the stellar populations found at those same regions. Wang, Höflich & Wheeler (1997) first suggested that there is a deficit of SN Ia in the central parts of galaxies, which was not observed for CC SNe. Ivanov, Hamuy & Pinto (2000) correlated SN properties with galactocentric radii and found that the range in brightness and light-curve width of SNe Ia increased with increasing radial distance from the centres of host galaxies, suggesting this was a progenitor age effect. Förster & Schawinski (2008) analysed the radial distribution of SN Ia in elliptical galaxies, finding that there was no statistical difference between the radial distribution of SN Ia and the light profile of their hosts. They concluded that this implied that some SN Ia progenitors do have delay times of several Gyr. More recently, Galbany et al. (2012) found that the average SN extinction and colour was correlated with radial position. Wang et al. (2013) have claimed that two distinct populations of SNe Ia exist, apparently implied from differences in the ejecta velocities of SNe found within the inner and outer regions of host galaxies. However, recently Pan et al. (2015) presented a separate analysis where the same trend was observed but with less significance.

To further investigate the local environments of SNe, one can analyse the properties of the stellar populations at the exact site of SNe. Kelly, Kirshner & Pahre (2008) employed pixel statistics (in a very similar fashion to that which we will use in the current analysis) finding that the SNe Ia population statistically followed the distribution of g'-band light of their hosts, in a similar fashion to SNe II. Comparing those statistics to an analytical model of spiral galaxy light distributions, Raskin et al. (2009) concluded that even the most 'prompt' SNe Ia have delay times of more than a few 100 Myr. Wang et al. (2013) found that SNe Ia with higher ejecta velocities fall on brighter regions of their hosts than those with lower measured velocities. In addition, Rigault et al. (2013) showed that SNe Ia occurring in regions with detected Hα emission are 'redder' than those exploding where no emission is found. Meanwhile, Galbany et al. (2014) published a study of SNe environments using integral field spectroscopy (IFS). They showed through a variety of indicators that SNe Ia were found to occur further from star-forming regions than CC SNe. In addition they found that the SNe Ia location properties were on average the same as those measured globally. It is clear that future IFS studies will be particularly revealing for SN environment analyses. Most recently Kelly et al. (2014) demonstrated that SN Ia falling on regions of high ultraviolet (UV) surface brightness and SF density, appear to show significantly lower Hubble residuals, hence improving the accuracy of a subset of SN Ia as distance indicators. This result was actually predicted in Childress, Wolf & Zahid (2014) who suggested that SN Ia selected exclusively from star-forming host galaxies would yield a more cosmologically uniform sample.

In summary, SN environment analyses to-date have shown some intriguing results, which despite the significant delay times of their progenitors, demonstrate that these types of studies can indeed be revealing for SNe Ia. As expected, SNe Ia explode in distinct environments to CC SNe (see e.g. initial study in James & Anderson 2006), confirming their older progenitors. There appears to be a deficit of SNe in the central regions of star-forming galaxies, which

perhaps implies that the old bulge populations of these galaxies are not significant producers of SNe Ia. Meanwhile, environment studies suggest that at least a significant fraction of SN Ia colour diversity is produced by host galaxy extinction, due to the preference of 'redder' SNe for more central regions and for higher Hα flux environments. There is also an intriguing suggestion that environments can be used to select SNe samples with lower Hubble residuals. However, the above also shows that environment studies are still somewhat in their infancy, particularly when compared to studies of light-curve properties. Investigations have generally concentrated on one specific measurement, and often suffer from insufficient statistics. Hence, a more wide ranging study of SN Ia environments which attempts to bring together many of the aspects of the above is warranted.

In the current paper we further investigate the properties of the immediate environments of SNe Ia within star-forming host galaxies, using multicolour host galaxy pixel statistics, and the radial distribution of events with respect to both SF and the older stellar continuum population. This follows from James & Anderson (2006) where a small sample of SNe Ia was analysed using these techniques.

The paper is organized as follows. In the next section we discuss the SN and galaxy samples, and summarize how we obtained our data and their reduction. In Section 3 the statistical methods we employ are discussed, and in Section 4 the results are presented. This is followed by a discussion of their implications for our understanding of SNe Ia transient and progenitor properties in Section 5. Finally, we summarize and list our main conclusions in Section 6.

2 SUPERNOVA AND HOST GALAXY SAMPLES

The sample we study is a compilation of SNe and their host galaxies from the literature. Initially, the sample was formed from SNe which had occurred within the Hα Galaxy Survey (HαGS; James et al. 2004), a representative survey of star-forming galaxies within the local Universe. Since the analysis of those data (James & Anderson 2006), a significantly larger sample of Hα and *R*- or r'-band host galaxy observations have been obtained. The only criterion for obtaining these data was that (a) host galaxies had recession velocities less than 6000 km s^{-1} so that we can probe distinct stellar populations;[1] (b) host galaxies had major to minor axis ratios of less than 4:1 to reduce issues with chance superpositions of foreground or background stellar populations on to SNe explosion sites; and (c) hosts were targeted where individual SNe had published photometry, so that light-curve parameters could be derived and compared to environmental information. Our initial aim to investigate the association of SNe Ia with SF within galaxies restricts our sample to star-forming late-type galaxies. Later we will analyse and discuss possible systematics that this may bring to our conclusions. The sample of SNe and their host galaxies is listed in Table 1, together with derived SN light-curve parameters. Before describing host galaxy observations, we outline the methods for extracting light-curve parameters for our sample using literature photometry.

2.1 Light-curve parameters

In addition to analysing the environments of SNe Ia as an overall population, it is also fruitful to analyse whether specific SN Ia properties show correlations with their environment. This is motivated by differences in SNe light-curve parameters found with global galaxy properties. Observables of individual SNe Ia can be extracted from their optical light curves. To proceed, literature photometric data were searched for all SNe in our sample. Where useful photometry was found we list the source in Table 1. We then use *SIFTO* (Conley et al. 2008), a light-curve fitter that uses spectral template time series that are adjusted to the observed colours of SN Ia photometry to obtain values of *B*-band maximum date, a light-curve width parameter or 'stretch' of the time-axis relative to the template, and multiplicative factors for each band from which an observed $(B-V)_{\rm max}$ colour is obtained. In order to include photometry in our analysis we require that for colour estimations at least one photometric point is available between -15 and $+8$ d, and one available between $+5$ and $+25$ d with respect to *B*-band maximum in both the *B* and *V* bands. In the case of stretch we include SNe if data are available in only one of these bands (or other filters). Furthermore, we only include light-curve fits which give stretch values in the range 0.4–1.6. Redshift and Galactic extinction are additional inputs to the fitter. The fitted colour is a combination of intrinsic colour and host reddening, for which no extinction law is applied. We recall that stretch is highly correlated with SN brightness, with higher stretch events being intrinsically brighter SNe (Perlmutter et al. 1997). The resulting light-curve parameters are listed in Table 1.[2]

2.2 Host galaxy observations

The principal aim of this work is to analyse the association of SNe Ia with SF within their host galaxies. To proceed with this aim we use our own Hα imaging, plus *Galaxy Evolution Explorer* (*GALEX*) near-UV imaging taken from the *GALEX* data base.[3] The original Hα imaging galaxy sample was taken from the HαGS. Additional data have since been obtained through various time allocations, and the sample we present here is of Hα plus *R*- or r'-band (henceforth we will refer to both of these as simply '*R*-band') imaging of 102 SN Ia host galaxies. In addition to Hα and near-UV imaging which we use to trace SF on differing time-scales, we also analyse host environment properties using *R*-band imaging together with *B*-band, plus *J*- and *K*-band near-infrared (IR) images. Next each data set which forms our sample is discussed in detail, documenting how they were obtained, their reduction, and finally what type of information can be gained by analysing host galaxy imaging at those specific wavebands.

2.3 Host galaxy Hα and *R*-band imaging

Hα line emission within galaxies traces regions of young on-going SF. The emission is produced from the recombination of interstellar medium (ISM) hydrogen atoms after ionization from the intense UV flux of young massive stars. The massive stars which make the dominant contribution to this ionizing flux are of $>$15–20 M$_{\odot}$, and therefore H II regions within galaxies are thought to trace SF of ages of less than $\sim$10 Myr (Kennicutt 1998). This is obviously much younger than even the most 'prompt' SN Ia scenarios (Aubourg

[1] A couple of slightly higher recession velocity host galaxies are included, but make no difference to the overall results presented in the paper.

[2] While it would seem interesting to correlate environmental information with Hubble residuals, once we make a redshift cut to the SNe with light-curve information (to remove the effect of galaxy peculiar velocities) the resulting sample is too small to apply such statistical tests as outlined here.

[3] http://archive.stsci.edu/index.html

Table 1. SN and host galaxy parameters. The SN sample analysed in this work, together with estimated light-curve parameters and references for photometry. In column 1 we list the SN name, followed by the host galaxy in column 2. Then in columns 3 and 4, respectively, we list the Hubble type and recession velocity of each host galaxy (information taken from NED: http://ned.ipac.caltech.edu/). This is followed by the derived light-curve parameters for each SN: stretch followed by $(B-V)_{\rm max}$ (the $B-V$ colour at maximum light). In column 7 we list the reference for SN photometric data (where we only include data if the light-curve fits passed our selection criteria).

SN	Host galaxy	Galaxy type	$V_{\rm r}$ (km s^{-1})	Stretch	$(B-V)_{\rm max}$	Photometry references
1937C	IC 4182	SAm	321	1.227	···	Pierce & Jacoby (1995)
1954B	NGC 5668	SAd	1577	···	···	···
1957A	NGC 2841	SAb	638	···	···	···
1963I	NGC 4178	SBdm	374	···	···	···
1963J	NGC 3913	SAd	954	···	···	···
1968E	NGC 2713	SBab	3922	···	···	···
1968I	NGC 4981	SABbc	1680	···	···	···
1969C	NGC 3811	SBcd	3105	···	···	···
1971G[a]	NGC 4165	SABa	1859	···	···	···
1972H[b]	NGC 3147	SAbc	2802	···	···	···
1974G	NGC 4414	SAc	716	···	···	···
1975A	NGC 2207	SABbc	2741	···	···	···
1979B	NGC 3913	SAd	954	···	···	···
1981B	NGC 4536	SABbc	1808	···	···	···
1982B	NGC 2268	SABbc	2222	···	···	···
1983U	NGC 3227	SAB	1157	···	···	···
1986A	NGC 3367	SBc	3040	···	···	···
1986G	NGC 5128	S0[c]	547	0.717	0.839	Phillips et al. (1987)
1987D	MCG +00-32-01	SBbc	2217	···	···	···
1987O	MCG +02-20-09	S	4678	···	···	···
1989A	NGC 3687	SABbc	2507	···	···	···
1989B	NGC 3627	SABb	727	0.940	0.394	Wells et al. (1994)
1990N	NGC 4639	SABbc	1018	1.064	0.041	Lira et al. (1998)
1991T	NGC 4527	SABbc	1736	1.068	0.082	Ford et al. (1993), Lira et al. (1998) Altavilla et al. (2004)
1991ak	NGC 5378	SBa	3042	···	···	···
1992G	NGC 3294	SAc	1586	···	···	···
1992K	ESO 269-G57	SABb	3106	···	···	···
1992bc	ESO 300-G09	Sab	5996	1.059	–0.089	Hamuy et al. (1996c)
1994S	NGC 4495	Sab	4550	1.030	–0.021	Riess et al. (1999)
1994ae	NGC 3370	SAc	1279	1.054	–0.050	Altavilla et al. (2004), Riess et al. (2005)
1995D	NGC 2962	SAB0	1966	1.089	0.033	Patat et al. (1996), Meikle et al. (1996) Altavilla et al. (2004)
1995E	NGC 2441	SABb	3470	0.958	0.679	Riess et al. (1999)
1995al	NGC 3021	SAbc	1541	1.074	0.107	Riess et al. (1999)
1996Z	NGC 2935	SABb	2271	0.915	···	Riess et al. (1999)
1996ai	NGC 5005	SABbc	946	1.097	1.553	Riess et al. (1999)
1997Y	NGC 4675	SBb	4757	···	···	···
1997bp	NGC 4680	Pec	2492	1.016	0.152	Jha et al. (2006)
1997bq	NGC 3147	SAbc	2802	0.917	0.031	Jha et al. (2006)
1997do	UGC 3845	SBbc	3034	0.975	0.018	Jha et al. (2006)
1997dt	NGC 7448	SAbc	2194	···	···	···
1998D	NGC 5440	Sa	3689	0.869	–0.046	Jha et al. (2006)
1998aq	NGC 3982	SABb	1109	0.986	–0.104	Riess et al. (2005)
1998bu	NGC 3368	SABab	897	0.974	0.269	Suntzeff et al. (1999)
1998dh	NGC 7541	SBbc	2689	0.939	0.088	Jha et al. (2006), Ganeshalingam et al. (2010)
1998eb	NGC 1961	SABc	3934	···	···	···
1999aa	NGC 2595	SABc	4330	1.113	–0.036	Altavilla et al. (2004), Jha et al. (2006)
1999bh	NGC 3435	Sb	5158	0.818	0.872	Ganeshalingam et al. (2010)
1999bv	MCG +10-25-14	S	5595	···	···	···
1999by	NGC 2841	SAb	638	0.618	0.484	Garnavich et al. (2004), Ganeshalingam et al. (2010)
1999cl	NGC 4501	SAb	2281	0.939	1.059	Krisciunas et al. (2006), Jha et al. (2006) Ganeshalingam et al. (2010)
1999cp	NGC 5468	SABcd	2842	0.994	–0.027	Krisciunas et al. (2000), Ganeshalingam et al. (2010)
1999gd	NGC 2623	Pec	5549	0.976	0.367	Jha et al. (2006)
2000E	NGC 6951	SABbc	1424	1.052	0.130	Valentini et al. (2003), Tsvetkov (2006) Lair et al. (2006)
2000ce	UGC 4195	SBb	4888	···	···	···
2001E	NGC 3905	SBc	5774	1.002	–0.023	Ganeshalingam et al. (2010)
2001ay	IC 4423	S	9067	1.600	···	Hicken et al. (2009)

Table 1 – *continued*

SN	Host galaxy	Galaxy type	V_r (km s^{-1})	Stretch	$(B-V)_{max}$	Photometry references
2001bg	NGC 2608	SBb	2135	0.935	0.171	Ganeshalingam et al. (2010)
2001cz	NGC 4679	SAbc	4643	1.006	0.090	Krisciunas et al. (2004)
2001eg	UGC 3885	S	3809	...	...	...
2002au	UGC 5100	SBb	5514	...	...	...
2002bs	IC 4221	SAc	2889	...	...	...
2002cr	NGC 5468	SABcd	2842	0.945	–0.013	Hicken et al. (2009)
2002er	UGC 10743	Sa	2569	0.930	0.138	Pignata et al. (2004), Ganeshalingam et al. (2010)
2002fk	NGC 1309	SAbc	2136	1.010	–0.093	Hicken et al. (2009)
2003cg	NGC 3169	SAa	1238	0.984	1.110	Elias-Rosa et al. (2006), Hicken et al. (2009) Ganeshalingam et al. (2010)
2003cp	MCG +10-12-78	Sb	5927	...	...	...
2003du	UGC 9391	SBdm	1914	1.019	–0.084	Leonard et al. (2005)
2004bc	NGC 3465	Sab	7221	...	...	...
2004bd	NGC 3786	SABa	2678	...	...	...
2005A	NGC 958	SBc	5738	0.977	0.986	Contreras et al. (2010)
2005F	MCG +02-23-27	S	8545	...	...	...
2005G	UGC 8690	Scd	6938	...	...	...
2005M	NGC 2930	S	7382	1.114	0.312	Stritzinger et al. (2011)
2005W	NGC 691	SAbc	2665	0.954	0.144	Stritzinger et al. (2011)
2005am	NGC 2811	SBa	2368	0.778	0.056	Contreras et al. (2010)
2005bc	NGC 5698	SBd	3679	0.830	0.377	Ganeshalingam et al. (2010)
2005bo	NGC 4708	SAab	4166	0.852	0.243	Ganeshalingam et al. (2010), Contreras et al. (2010)
2005cf	MCG −01-39-03	S0[d]	1937	0.995	–0.015	Wang et al. (2009)
2005el	NGC 1819	SB0[e]	4470	0.886	–0.088	Contreras et al. (2010)
2005ke	NGC 1371	SABa	1463	0.677	0.653	Hicken et al. (2009), Stritzinger et al. (2011)
2006D	MCG −01-33-34	SABab	2556	0.818	0.105	Stritzinger et al. (2011)
2006N	MCG +11-08-12	?	4280	0.795	0.027	Hicken et al. (2009)
2006X	NGC 4321	SABbc	1571	0.995	1.196	Stritzinger et al. (2011)
2006ax	NGC 3663	SAbc	5018	0.984	–0.089	Hicken et al. (2009), Stritzinger et al. (2011)
2006ce	NGC 908	SAc	1509	...	...	...
2006mq	ESO 494-G26	SABb	968	...	...	...
2006ou	UGC 6588	Sbc	4047	1.393	0.345	Hicken et al. (2012)
2007N	MCG −01-33-12	SAa	3861	0.524	0.988	Hicken et al. (2009), Stritzinger et al. (2011)
2007S	UGC 5378	Sb	4161	1.095	0.116	Hicken et al. (2009), Stritzinger et al. (2011)
2007af	NGC 5584	SABcd	1638	0.953	0.073	Hicken et al. (2009), Stritzinger et al. (2011)
2007bm	NGC 3672	SAc	1862	0.922	0.474	Hicken et al. (2009), Stritzinger et al. (2011)
2008bi	NGC 2618	SAab	4031	...	...	...
2008fv	NGC 3147	SAbc	2802	1.104	0.165	Tsvetkov & Elenin (2010), Biscardi et al. (2012)
2009ag	ESO 492-G02	SAb	2590	0.978	0.124	Unpublished, Carnegie Supernova Project
2009ds	NGC 3905	SBc	5774	1.144	0.073	Hicken et al. (2012)
2009ig	NGC 1015	SBa	2629	1.075	0.140	Foley et al. (2012a), Hicken et al. (2012)
2010eb	NGC 488	SAb	2272	...	...	...
2011B	NGC 2655	SAB0/a	1400	...	...	...
2011ao	IC 2973	SBd	3210	...	...	...
2011ek	NGC 918	SABc	1507	...	...	...
2011dm	UGC 11861	SABdm	481	...	...	...
2011dx	NGC 1376	SAcd	4153	...	...	...

Notes. [a]Classification from IAU SN catalogue.
[b]Classification as SN Ia from Sandage & Tammann (1993).
[c]While this galaxy is classed as Hubble type S0 (i.e. no, or very little SF), there is definitely large amounts of detected Hα line emission produced by on-going SF.
[d]Galaxy is classified as S0, but significant on-going SF is detected.
[e]Galaxy is classified as S0, but significant on-going SF is detected.

et al. 2008). However, it will be shown that an investigation into the association of SNe Ia with these regions can still produce interesting results.

The narrow-band Hα imaging technique involves observing through a narrow Hα filter (on the order of 50–100 Å) together with separate broad-band imaging to remove the continuum. Here, we use R or r' filters to remove this component. This also allows us to use these images for further analysis. The initial data used for this project (imaging from HαGS; James et al. 2004) were obtained with the 1.0-m Jacobus Kapteyn Telescope (JKT), with a pixel scale of 0.333 arcsec pixel^{-1}. In the first paper of the current series (James & Anderson 2006), data and analysis were published for 12 SN Ia host environments. Here we significantly increase this sample size. Hα and R-band imaging data were obtained with the Wide Field Camera (WFC; 0.333 arcsec pixel^{-1} image scale) mounted on the Isaac Newton Telescope (INT) over the course

of two observing runs during 2007 February and 2008 February. In addition, we searched through a series of previous INT data samples taken for other projects by coauthors of the current paper for further host galaxy imaging. During various time allocations between 2005 and 2009 host galaxy Hα and r'-band imaging was obtained with RATCam on the Liverpool Telescope (LT; Steele et al. 2004), with a pixel scale of 0.278 arcsec pixel^{-1}. Most recently Hα and *R*-band data were obtained with the Max Planck Gesellschaft (MPG)/European Southern Observatory (ESO) 2.2-m telescope together with the Wide Field Imager (WFI; Baade et al. 1999) during 2010 February. WFI has a pixel scale of 0.238 arcsec pixel^{-1}.

While the exact details of observing strategy changed slightly between different telescopes and instruments, overall procedures were very similar. Generally three 300-s Hα exposures were obtained, followed by one 300-s broad-band *R*-band image. Standard imaging reduction techniques were employed using IRAF[4] to first bias-subtract then flat-field all science frames. A range of foreground stars were then used to obtain a scaling factor between the narrow and broad-band observations. After scaling, the broad-band images were subtracted from the Hα observations. This leaves only the Hα line emission within host galaxies, ready for analysis. Finally, images were astrometrically calibrated using the STARLINK package ASTROM, enabling sub-arcsecond location of the SN explosion sites.

2.4 *GALEX* data

Hα line emission within galaxies traces the most recent, on-going SF regions of ages less than 10 Myr. Given that this is a much shorter time-scale than even the youngest hypothesized SN Ia progenitors, we also choose to investigate the association of SN Ia explosion sites with SF of older ages. Near-UV emission within galaxies is thought to trace SF out to older ages ($\sim$100 Myr; see e.g. Gogarten et al. 2009). In the rest of the paper we will refer to near-UV imaging as tracing recent SF (in place of on-going with respect to that traced by Hα). We searched the *GALEX* archive for near-UV images of our sample. Data were available for 74 SN Ia host galaxies and *GALEX* near-UV 'intensity maps' were obtained, which come astrometrically calibrated ready for analysis. These data have scales of 1 arcsec pixel^{-1}.

2.5 INT *B*-band data

B-band imaging was obtained with the WFC on the INT. Exposure times of $\sim$500 s were employed and the WFC gives images of 0.333 arcsec pixel^{-1} scale. Standard imaging reduction techniques were employed to first bias-subtract then flat-field all science frames. Images were then astrometrically calibrated and accurate SN positions on reduced images were obtained.

2.6 NOT near-IR data

To obtain near-IR *J*- and *K*-band imaging the Nordic Optical Telescope (NOT) was employed using NOTCam. The instrument was used in wide field imaging mode which results in images with a field of view of 4 $\times$ 4 arcmin^2 and a pixel scale of 0.234 arcsec pixel^{-1}. A total *J*-band exposure time of 200 s was used, split into 4 $\times$ 50 s exposures. To account for the varying near-IR sky, frames offset from host galaxies were observed with the same exposure times as those used for science frames. Therefore 50-s exposures were taken on target, then offsets of 250 arcsec were applied to slew to sky positions. Within this sequence positions were dithered by 10 arcsec to remove stars from the sky frames and bad pixel defects on the detector. A similar process was employed for the *K*-band images with a total exposure time of 900 s split into 9 $\times$ 100 s exposures. Differential flat-fields were obtained at either the start or the end of each observing night. Sky flats with low count levels were subtracted from similar frames with high levels and then the resulting flat-field was normalized. Each subsequent sky frame was subtracted from its corresponding science frame. Each resulting sky-subtracted science frame was then divided by the normalized flat-field. These resulting frames were then combined using median stacking. Images were then astrometrically calibrated as above. However, in many cases there were insufficient stars within the relatively small field of view of NOTCam to enable an astrometric solution. In these cases SN positions were calculated using offsets of SN coordinates from galaxy centres [with SN positions being taken from either the IAU SN list or NASA/IPAC Extragalactic Database (NED), and galaxy centre coordinates taken from NED]. Offsets were transformed to NOTCam pixel x and y offsets, and SN positions on the images were calculated using the peak of the *J*- or *K*-band flux on each image as the galaxy centre. To check the validity of this process, SN positions were also calculated in this way for images where an astrometric calibration was possible and the two methods were compared. In general SN pixel positions were consistent between the two methods, and NCR values (see below) were also consistent between the two pixel coordinate values. The difference in the mean NCR values between the 21 SNe where the above comparison was possible in the *J*-band is 0.008, while for 20 SNe in the *K*-band the difference is 0.023.

2.7 Stellar populations traced by different wavebands

In this work we analyse the association of SNe Ia within star-forming hosts with galaxy light distribution in a range from Hα through optical wavebands to *K*-band near-IR observations. Each waveband analysed (Hα, near-UV, *B*-, *R*-, *J*-, and *K*-band) traces different stellar population properties. Hα emission traces SF on the shortest time-scales of less than $\sim$10 Myr. Near-UV emission traces SF on longer time-scales out to $\sim$100 Myr. When one moves to analyse broad-band observations at longer wavelengths direct age constraints become less clear. However, stellar population models appear to be in agreement that as one moves redwards then the older stellar mass of a stellar population/galaxy starts to contribute more significantly (see e.g. Worthey 1994; Schawinski et al. 2007 who used the models of Maraston 2005). While it is generally assumed that young populations still dominate the flux detected through the *B*-band filter, the *K*-band light in most stellar populations is assumed to be dominated by the old stellar mass of that population (e.g. Mannucci et al. 2005).[5] Following the above, we can speculate that if a SN distribution better traces that flux observed through a redder filter, then the dominant age of the progenitor population may be larger than that of a distribution which traces flux observed through a bluer filter. The above is obviously only a first-order approximation, and one should be careful to draw strong conclusions following these arguments, especially given the

[4] IRAF is distributed by the National Optical Astronomy Observatory, which is operated by the Association of Universities for Research in Astronomy (AURA) under cooperative agreement with the National Science Foundation.

[5] While Kangas et al. (2013) claimed that the *K*-band light in their galaxy sample may be tracing recent SF, this was due to their sample being of IR-bright starburst galaxies, significantly distinct from the current sample.

effects of metallicity and extinction. However, in the following sections we will use this argument as a guide to understand the distributions derived, while stressing the uncertainties involved. In Section 5.1.1 we present further constraints on the stellar population properties probed by our broad-band images.

3 ANALYSIS METHODS

The procedures for obtaining results from the statistical methods we use here, were first presented in James & Anderson (2006), and have been further outlined in their application to CC SN host galaxy samples in Anderson & James (2008, 2009), Habergham, Anderson & James (2010), Anderson et al. (2012), Habergham, James & Anderson (2012), and Habergham et al. (2014). Below we briefly outline our methods, but refer the reader to those previous publications for more detailed documentation.

3.1 Pixel statistics

In James & Anderson (2006), a pixel statistics method was introduced which was created to give a quantitative measure of the association of individual SNe to the underlying SF present within galaxies. This method produces for each pixel within an image a value (dubbed 'NCR'; Anderson & James 2008) between 0 and 1 which indicates where within the overall host galaxy SF distribution each pixel is found (note a very similar technique was independently developed by Fruchter et al. 2006). Images are first trimmed to remove non-galaxy regions of the field of view, and are then binned 3×3 (in order to reduce the effects of inaccurate SN coordinates and/or image alignment).[6] Pixels within each image are then ordered in terms of increasing count. From this ordered list we then form the cumulative distribution. Each pixel is then assigned an 'NCR' value by dividing the cumulative pixel count by the total of the cumulative distribution. All pixels forming part of the negative cumulative distribution are set to an NCR value of zero (either sky or zero flux pixels). Hence, all pixels have a value between 0 and 1, where a value of 0 indicates that the pixel is consistent with zero flux or sky values, whereas a pixel value of 1 means that the pixel has the highest flux count within the image. To build up NCR statistics for SN populations one simply takes the pixel where each SN falls and calculates its corresponding NCR value.

In the case of the current sample we apply this technique to each SN with respect to its Hα image, and in addition with respect to its *GALEX* near-UV image, broad-band optical *B* and *R* images, and near-IR *J*- and *K*-band images. The resulting NCR values are listed in Table A1. Any population which directly follows the spatial distribution of light traced by each waveband will show a flat distribution of NCR values with a mean value of 0.5. Whether a distribution follows such an one-to-one relation or not, then provides constraints on progenitor properties. In the cumulative plots below if a distribution accurately traces the light detected through a given filter, then one expects the distribution to follow the diagonal one-to-one line shown on each plot.

3.1.1 Spatial resolution

During the above description of our data sets, we have detailed the pixel scale of each distinct set of observations. During our processing of the host galaxy images, most data are binned 3×3 which means all images (UV through to near-IR) have NCR values which probe counts at a detector resolution of $\sim$1 arcsec. However, in some cases the seeing during observations was considerably worse than this. Of all observations the image quality in the *B*-band was the worst, hence we use these data to present a limiting case of the spatial resolutions probed within galaxies through our NCR statistic. The median seeing as measured on *B*-band images was 1.6 arcsec. The median recession velocity of our galaxy sample is 2647 km s^{-1}, which equates to a distance 36.3 Mpc. These two values give a median spatial resolution probed within galaxies of $\sim$280 pc. Hence, we resolve SN Ia host galaxies into a significant number of elements through our pixel statistics.

[6] As the near-UV images have an initial pixel scale of 1 arcsec pixel^{-1}, these data were not binned.

3.2 Radial analysis

While pixel statistics can give one information on the stellar population at exact explosion sites, SNe Ia have significant delay times and hence are likely to explode at considerable distances from their birth sites. One method to further explore the environments of SNe is to investigate where they explode with respect to the radial distribution of different stellar populations. Within star-forming galaxies different age and metallicity stellar populations are found at different characteristic galactocentric radial positions. Therefore one can investigate where SNe are found within these more generalized galaxy trends, and further infer progenitor properties.

In James & Anderson (2006) we introduced a statistical radial analysis of host galaxies, which compares the radial distribution of SNe to those of stellar populations as traced by the continuum *R*-band light and the Hα emission, respectively. To obtain these 'Fr' fractional flux values one proceeds in the following fashion. For each host galaxy elliptical apertures of increasing size are produced, centred on the galaxy central coordinates, and calculated using the position angle and ratio of major to minor axis of the galaxy (taken from NED). One then finds the aperture which just includes the SN position. The flux (both of the narrow- and broad-band emission) within that aperture is then calculated, and normalized to the total galaxy emission by dividing by the flux within an aperture where the cumulative flux of the galaxy has become constant as one goes to larger galactocentric radii. Hence, each SN has a radial value corresponding to the continuum *R*-band light (Fr_R), and one corresponding to Hα emission ($\mathrm{Fr}_{\mathrm{H}\alpha}$) between 0 and 1. A SN having a Fr value 0 would indicate that the SN exploded at the central peak Hα or *R*-band pixel of the galaxy, while a value of 1 means that the SN falls on an outer region where the galaxy flux is negligible above the sky. Fr_R and $\mathrm{Fr}_{\mathrm{H}\alpha}$ SN Ia distributions are hence built. If a SN population directly follows the radial distribution of the broad- or narrow-band light, then the distribution of Fr values is expected to the flat. Therefore, we can investigate how the different samples are associated with the radial positions of different stellar populations. These techniques have been applied to CC SN samples in Anderson & James (2009) and Habergham et al. (2010, 2012, 2014).

4 RESULTS

4.1 Pixel statistics

4.1.1 Hα

We present the overall SNe Ia Hα NCR pixel distribution with respect to other main SN types in Fig. 1 (note, an in-depth analysis of the CC SN sample was presented in Anderson et al. 2012). It

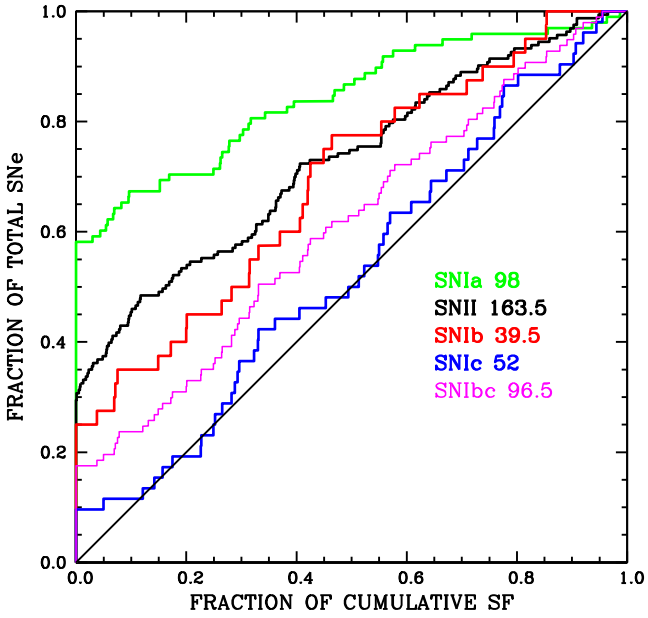

Figure 1. Cumulative Hα pixel statistics distributions of the main SN types. As distributions move away to the upper left from the black diagonal (a hypothetical distribution, infinite in size, that accurately traces the underlying on-going SF), they are showing a lower association with the emission. (We note that this plot is the same as that presented in Anderson et al. 2012.)

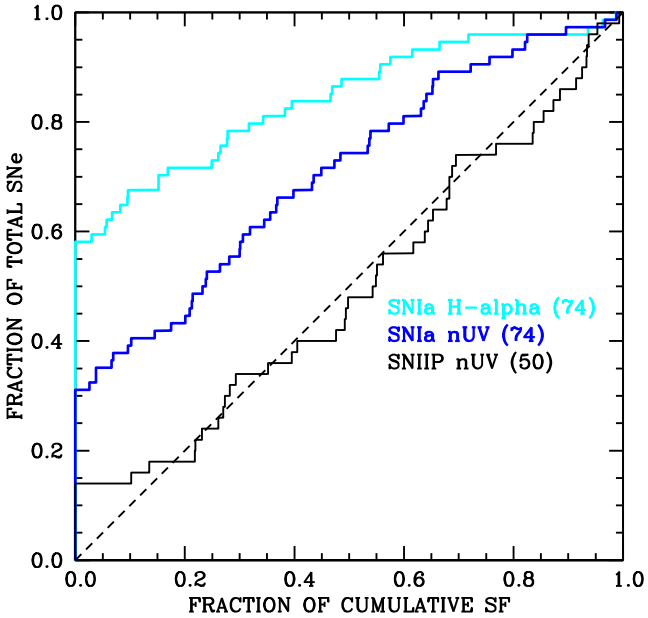

Figure 2. Cumulative distribution NCR plot showing the SN Ia population with respect to Hα and near-UV emission of their host galaxies. For reference the SN IIP distribution with respect to near-UV emission is shown in solid black (taken from Anderson et al. 2012).

is immediately apparent that SNe Ia show the lowest degree of association with the on-going SF (as seen previously by Bartunov, Tsvetkov & Filimonova 1994; James & Anderson 2006 and most recently by Galbany et al. 2014). This is to be expected if, as generally assumed, SNe Ia arise from some system containing a WD, i.e. a relatively old progenitor population. The mean Hα NCR value (98 events)[7] is 0.157, with a standard deviation of 0.253, and a standard error on the mean of 0.026. This compares to mean values of 0.254 (162.5 SNe), 0.303 (40.5), and 0.469 (52) for the SN II, SN Ib, and SN Ic distributions, respectively. Nearly 60 per cent of SNe Ia within star-forming galaxies fall on zero Hα flux (down to the limits of our observations; see Anderson et al. 2012). Using a Kolmogorov–Smirnov (KS) test we find that there is less than a 0.1 per cent probability that the SN Ia and SN II distributions are drawn from the same parent population. The SN Ia distribution does not follow the on-going SF within galaxies. Given that Hα emission is generally thought to be produced from the ionizing flux from stars less than 10 Myr old (Kennicutt 1998), this result is consistent with even the youngest predicted time-scales for SN Ia progenitors (see e.g. Aubourg et al. 2008).

4.1.2 Near-UV

In Fig. 2 the cumulative NCR distributions are shown for 74 SNe Ia, with respect to both Hα and *GALEX* near-UV emission. The SN Ia distribution shows a higher degree of association with the UV emission than that of Hα. However, it still appears that SNe Ia do not accurately trace recent SF. The mean near-UV NCR value is 0.292 with a standard deviation of 0.292 and a standard error on the mean of 0.034. This compares to a mean Hα NCR value for the same 74 events of 0.175 (standard deviation of 0.224, standard error on the mean of 0.026). Using a KS test we find that there is a 0.5 per cent chance that the SN Ia distribution shows the same degree of association with both the Hα and near-UV emission. We also find that there is less than 0.5 per cent chance that the SN Ia and SN IIP distributions, with respect to the near-UV emission, are drawn from the same parent population. Finally, the SN Ia near-UV distribution has a less than 0.1 per cent chance of being drawn from a flat distribution, i.e. one that accurately traces the recent SF. This result suggests that at least the majority of SNe Ia found within star-forming galaxies do not explode on the time-scales of $<$100 Myr traced by near-UV emission (Gogarten et al. 2009).

4.1.3 Multiwaveband NCR statistics

In Fig. 3 we present the NCR distributions of SNe Ia for multiple wavelength observations. The mean NCR values together with KS test results of each distribution between that waveband and a flat distribution are presented in Table 2. The SN Ia population best traces the *B*-band host galaxy light, followed by the *R*-band light distribution. The SN Ia population does not follow the host galaxy light distribution in Hα, near-UV, nor the *J* and *K* bands. We speculate that this indicates that the SN Ia progenitor population in spiral galaxies does not arise from either the very young populations of less than a few 100 Myr (that traced by Hα and near-UV emission), but neither is it dominated by long lived population of several Gyr (i.e. that traced by the *J*- and *K*-band light). The fact that the SN Ia population most closely follows the *B*-band light indicates that the progenitor population in late-type galaxies is dominated by relatively young systems.

It is also interesting to note how the different waveband distributions compare to each other with respect to the values of individual SNe. Using the Pearson's test for correlation, we find that nearly all

[7] Note that not all SNe in the sample have both NCR and Fr values, hence this value is lower than the 102 stated for the full sample of events earlier.

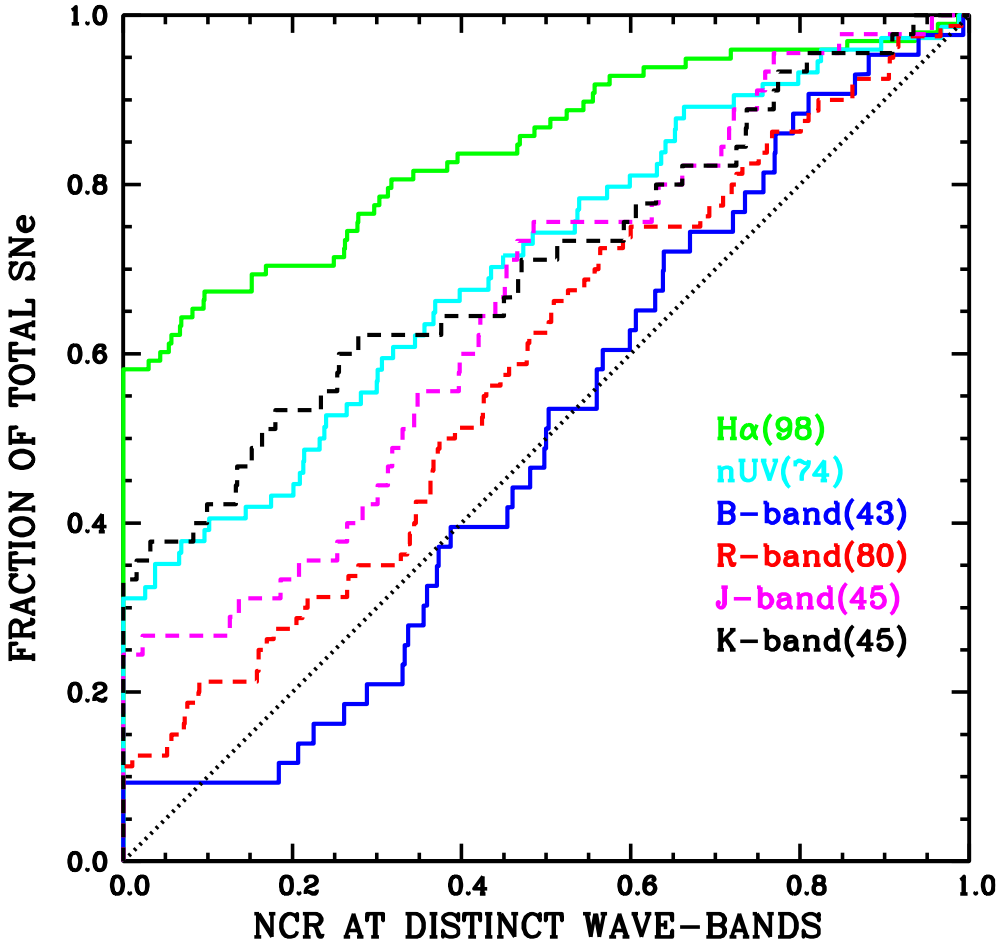

Figure 3. NCR distributions for SNe Ia with respect to six different waveband host galaxy images (in star-forming galaxies).

Table 2. NCR statistics for the six distinct waveband analyses. In column 1 the waveband is indicated, followed by the number of SNe and host galaxies analysed in column 2. In column 3 the mean NCR value for each distribution is presented. Finally, in column 4 the chance possibility of each distribution following a flat distribution is listed, as calculated using the KS test. (Note, if we only analyse those SNe common to all wavebands, the results are completely consistent with the below.)

Imaging band	Number of SNe	Mean NCR	KS test from flat distribution
Hα	98	0.157	<0.1 per cent
near-UV	74	0.292	<0.1 per cent
B	43	0.498	>10 per cent
R	80	0.415	~5 per cent
J	45	0.345	~0.5 per cent
K	45	0.293	<0.1 per cent

wavebands NCR values show significant correlation.[8] This means that if a SN has an NCR value near the top (or bottom) of the distribution in e.g. the *R* band, then it is likely to have an NCR value near the top (or bottom) of the distribution in e.g. Hα, although the absolute NCR values may be significantly offset. The only wavebands that do not show significant correlation are *K* and near-UV; *K* and Hα; and perhaps surprisingly near-UV and Hα. While a full discussion of the significance of these trends is beyond the scope of this paper, one may speculate that this indicates that while there are differences between the stellar populations traced by these different observations, the populations cluster together, i.e. where one finds significant flux of stellar light (e.g. *B* and *R* band) one also finds peaks of SF (Hα and near-UV). An analysis comparing pixel statistics between different wavebands, and including all host galaxy pixels (i.e. not just those where SNe have exploded), may give interesting constraints galaxy SFHs. Such analysis, independent of SN studies, will be the focus of future work.

[8] Where we define significant correlation as a Pearson's *r*-value higher than 0.5.

4.1.4 *Hα pixel statistics with respect to event properties*

SNe Ia light-curve stretch values were estimated for 56 SNe within the sample, as outlined in Section 2.1. We split this sample by the median stretch of 0.978 and resulting Hα NCR cumulative distributions are shown in Fig. 4. No statistical difference between the two distributions is found. We were able to estimate $(B-V)_{\rm max}$ values for 54 SNe and the sample is split by the median $(B-V)_{\rm max}$ value of 0.111. The results from this analysis are presented in Fig. 5. 'Redder' events (those with $(B-V)_{\rm max} > 0.111$) show a higher degree of association with Hα than 'bluer' SNe (similar to the results found by Rigault et al. 2013). The mean Hα NCR for the 'red' events is 0.209 (0.266, 0.052), while for the 'blue' events

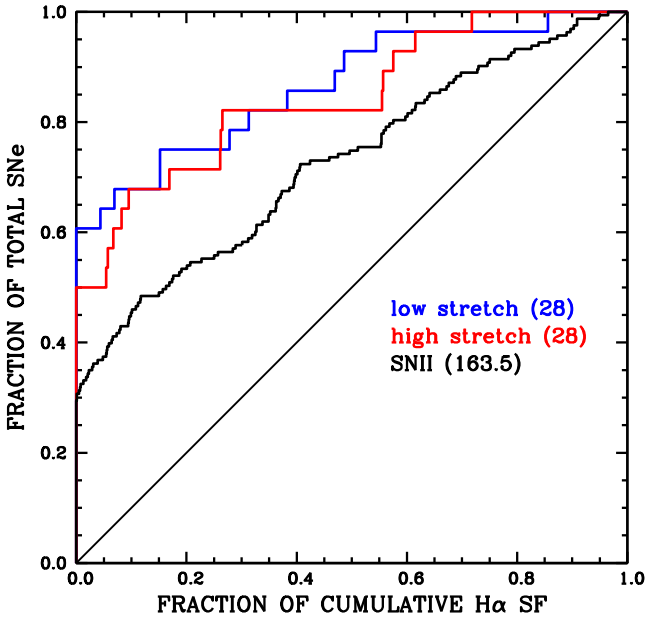

Figure 4. Hα cumulative pixel statistics plot with SNe Ia (in star-forming galaxies) split into those above and below the median stretch value of 0.978. The SN II distribution is shown for reference.

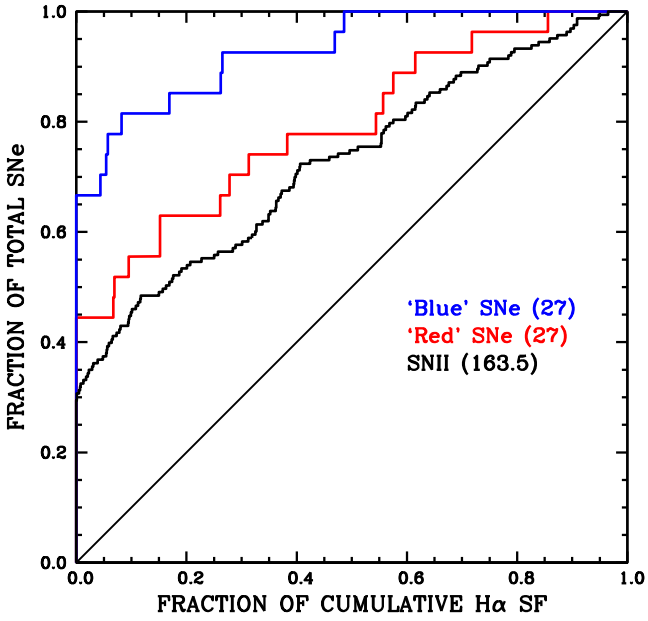

Figure 5. Hα cumulative pixel statistics plot with SNe Ia (in star-forming galaxies) split into those above and below the median $(B-V)_{\rm max}$ of 0.111. For reference the SN II distribution is also shown.

the mean is 0.070 (0.140, 0.027). Using a KS test, this difference is significant at the ∼10 per cent level (in addition the mean values are different at the 3σ level). An underlying difference in the sense that 'redder' SNe Ia are more likely to be found nearer/within bright H II regions could be explained by the fact that within bright H II regions SNe are likely to suffer from higher degrees of line-of-sight extinction. It is also possible that progenitor properties could play some role.

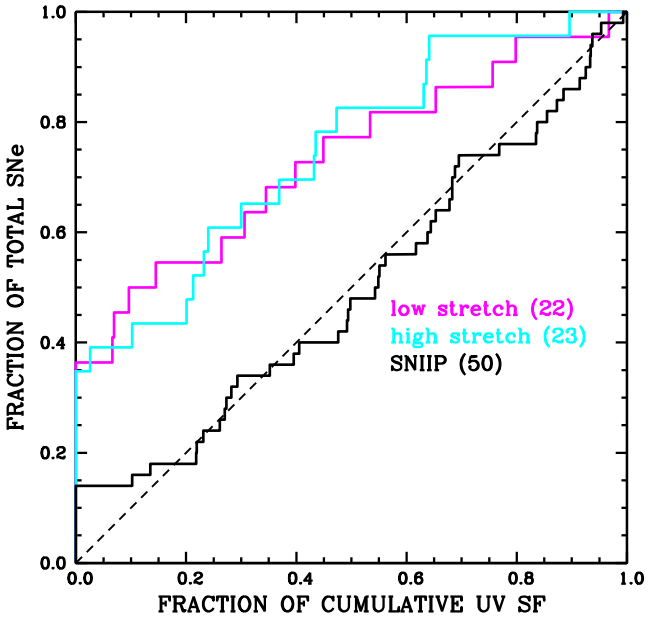

Figure 6. *GALEX* near-UV cumulative pixel statistics plot with SNe Ia (in star-forming galaxies) split into those above and below the media stretch value of the sample of 0.984. The SN IIP distribution (with respect to near-UV emission) is shown for reference.

4.1.5 Near-UV pixel statistics with respect to event properties

Now we repeat the analysis presented in the previous section but with respect to near-UV in place of Hα emission. There are some host galaxies within our Hα sample that do not have corresponding near-UV images available. Therefore for this subsample with available images we recalculate median stretch and $(B-V)_{\rm max}$ values, finding 0.984 and 0.105, respectively. The mean near-UV NCR values for the stretch distributions are 0.253 (0.267, 0.057) and 0.266 (0.307, 0.067) for the high and low stretch SNe, respectively, i.e. we find no statistical difference between the association of low and high stretch to recent SF, as shown in Fig. 6. This suggests that even the most 'prompt' SNe Ia found within star-forming galaxies – which are likely to be related to the higher stretch population – do not have delay times less than a few 100 Myr. The $(B-V)_{\rm max}$ distributions when split by the median value of 0.105 are shown in Fig. 7. It appears that 'redder' events show a higher degree of association with the near-UV emission than the 'bluer' ones. Again this trend is probably most easily explained by these SNe suffering from higher extinction from line-of-sight material, but we stress the possibility of progenitor properties playing some role. Below we further investigate the environments of the 'reddest' events in our sample. We note that if we repeat the above analysis with respect to the other wavebands analysed above we do not observe any significant differences between the stretch or colour samples.

4.2 Radial analysis

Here we present results from the fractional radial analysis, the methods for which were outlined in Section 3. We ask two main questions. (1) Does the radial distribution of SNe Ia within host galaxies accurately trace the *R*-band stellar continuum population, or more accurately the Hα emission, a tracer of the on-going SF within host galaxies? (2) If we split the SN Ia distribution by light-curve parameters, do specific types of SNe Ia occur at different characteristic

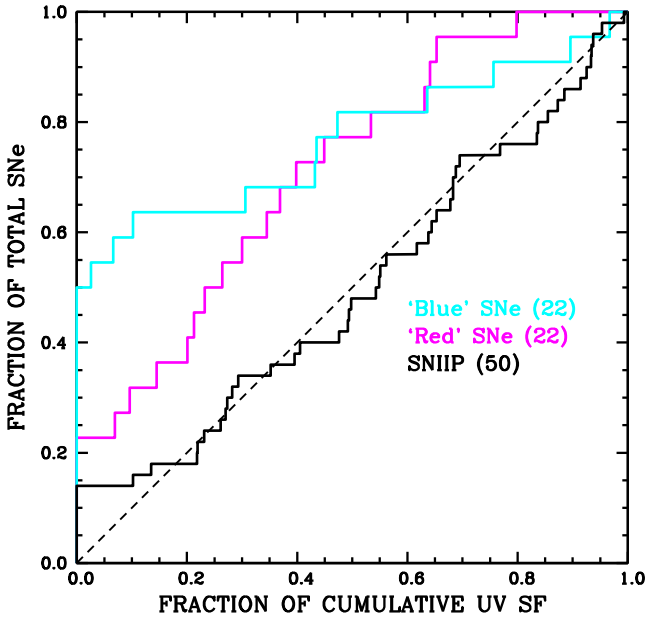

Figure 7. *GALEX* near-UV cumulative pixel statistics plot with SNe Ia (in star-forming galaxies) split into those above and below the median $(B-V)_{\rm max}$ of 0.105. The SN IIP distribution is shown for reference.

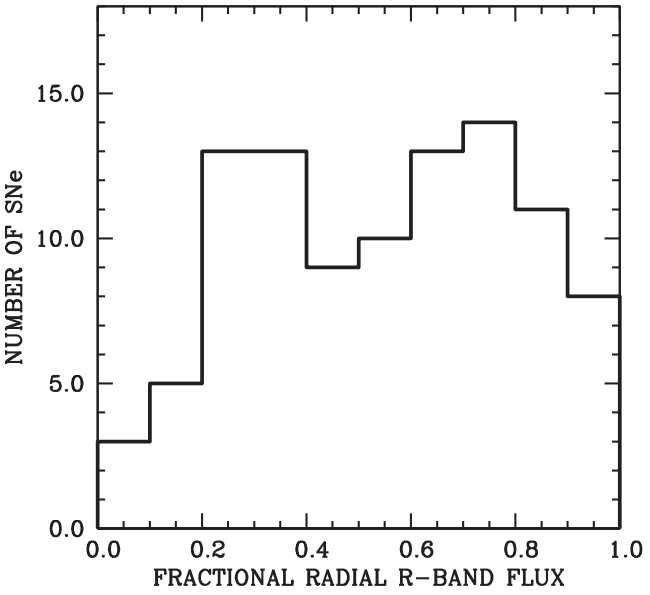

Figure 8. Histogram of fractional radial distribution of the overall SN Ia population (99 SNe in star-forming galaxies) with respect to the *R*-band light distribution of their hosts.

radial positions within galaxies? We start by analysing the overall radial distributions.[9]

4.2.1 *Overall SN Ia radial distributions*

In Fig. 8 a histogram of the radial distribution of SN Ia with respect to the stellar continuum of their hosts is presented. The mean Fr_R for the overall SN Ia distribution (99 SNe) is 0.554 (standard deviation of 0.261, standard error on the mean of 0.026). Hence, the distribution appears to be slightly biased towards larger radial distances when compared to the *R*-band light. There appears to be a central deficit of SNe Ia, and indeed this deficit is seen when we apply a KS test between the SN Ia Fr_R and a flat distribution. We find a ∼7 per cent chance that the SNe Ia accurately trace the radial *R*-band distribution of their hosts. The easiest way to interpret this result would be that it is solely a selection effect where SNe Ia go undetected in the central parts of galaxies due to higher levels of extinction and higher surface brightness. However, in Fig. 9 we show the SN Ia Fr_R, plot in a cumulative distribution, compared to that of 185 SNe II and 97 SNe Ibc (these results have been presented in Anderson & James 2009; Habergham et al. 2010, 2012). This shows that while the SNe II also have a central deficit, SNe Ibc do not show any such deficit. Given that SNe Ia are generally more luminous than SNe Ibc (meaning that any selection effect against finding SNe in the central parts of galaxies should be worse for the latter), this suggests that the lack of SNe Ia found within the central parts of galaxies is a real, intrinsic observation.

In Fig. 10 we show a histogram of the radial distribution of SNe Ia compared to the distribution of on-going SF of their hosts.

[9] We do not present Fr distributions with respect to the other wavebands analysed through our NCR method above. While pixels statistics give specific information at the exact location of each SNe, the Fr analysis is a much more crude environment property estimator, where differences between similar wavelength observations are not significant. In order to not overload the reader with additional analysis and figures we choose present only the Hα and *R*-band analysis in this section.

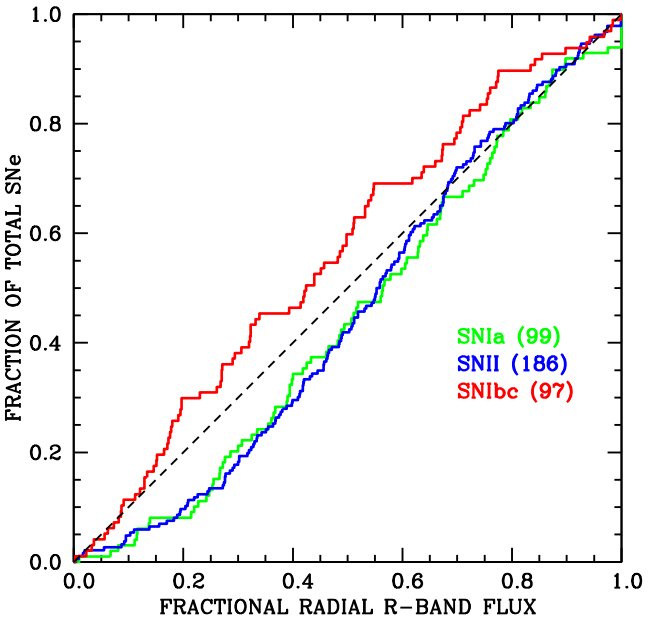

Figure 9. Cumulative distribution of the Fr_R values of SNe Ia (in star-forming galaxies) and the CC SN types, SN II and SN Ibc, with respect to the *R*-band light distribution within their host galaxies.

The mean $\mathrm{Fr}_{\mathrm{H}\alpha}$ is 0.560 (0.313, 0.031). As for the distribution with respect to the *R*-band light, the SNe Ia appear to explode at slightly larger galactocentric distances with respect to Hα emission. However, there is no large deficit in the central parts of the emission. This is also seen using a KS test where the SN Ia distribution is consistent with being drawn from a flat distribution, i.e. one that accurately traces the radial distribution of Hα emission. In Fig. 11 the SN Ia radial Hα cumulative distribution is presented, compared to that of 185 SNe II and 97 SNe Ibc. SNe Ia appear to become more numerous per unit SF out to larger galactocentric radii than the CC SNe within our previously published samples.

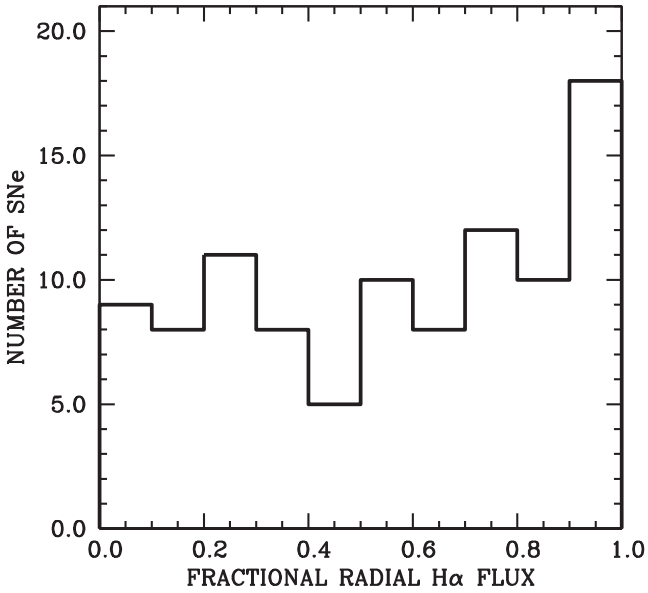

Figure 10. Histogram of fractional radial distribution of the overall SN Ia population (99 SNe in star-forming galaxies) with respect to the Hα line emission distribution of their host galaxies.

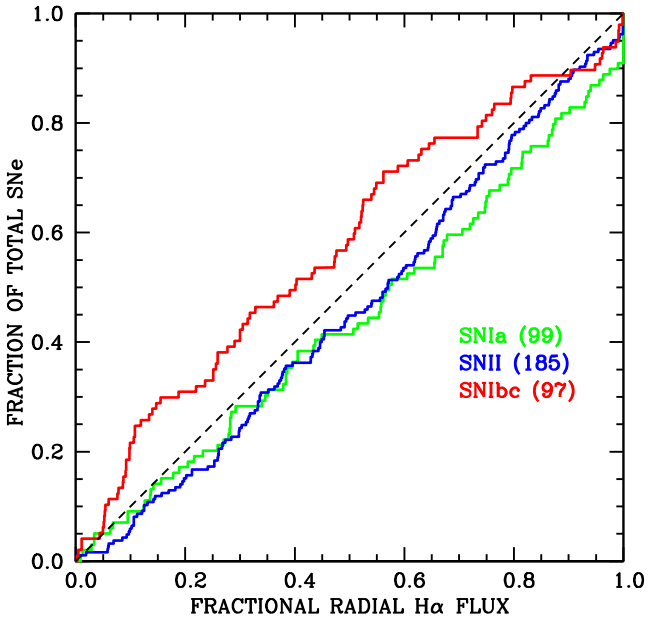

Figure 11. Cumulative distribution of the radial distribution of SNe Ia (in star-forming galaxies) and the CC SN types, SN II and SN Ibc, with respect to the Hα emission distribution within their host galaxies.

4.2.2 Radial distributions of SNe Ia when split by light-curve parameters

As was done for the pixel statistics analysis above, we now analyse whether there are differences in the radial distributions of SNe Ia when the sample is split by light-curve parameters. The sample is split by a median stretch of 0.984, and by the median $(B-V)_{\rm max}$ of 0.106. In Figs 12 and 13 histograms of the radial distributions of SNe Ia with respect to the *R* band and Hα light are shown, with the sample split by stretch. In Figs 14 and 15 histograms of the radial distributions are presented with the sample split by $(B-V)_{\rm max}$. The mean values (together with standard deviations and standard errors

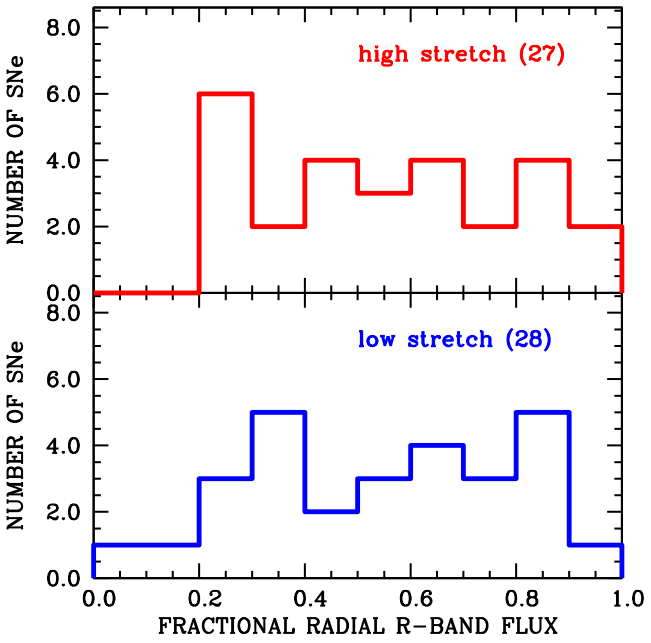

Figure 12. Histogram of fractional radial distribution of the SN Ia population (in star-forming galaxies) with respect to the *R*-band light distribution of their host galaxies, when split by the median stretch value of 0.984.

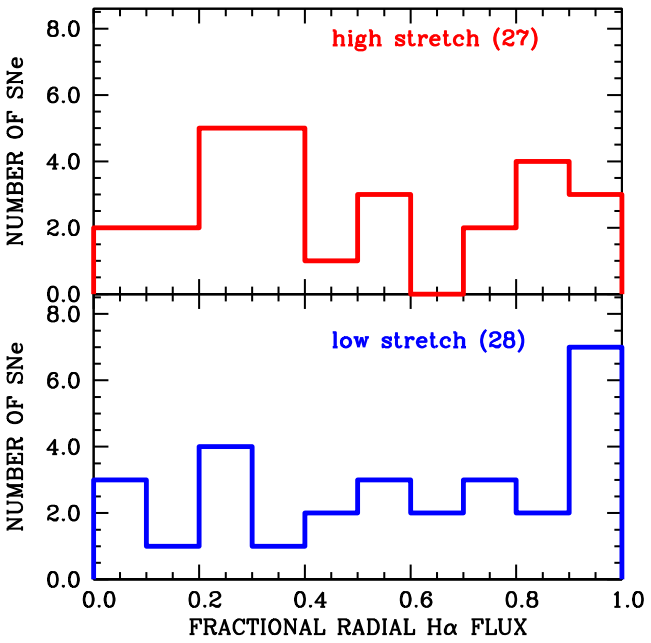

Figure 13. Histogram of fractional radial distribution of the SN Ia population (in star-forming galaxies) with respect to the Hα emission distribution of their host galaxies, when split by the median stretch value of 0.984.

on the mean), plus KS test percentage values, and sigma differences between means are listed in Table 3.

The most significant difference between these various populations is between the Fr_R distributions when split by SN colour. A KS test shows the distributions to be different with a 0.3 per cent chance probability of being drawn from the same underlying population. This difference is in the sense that 'redder' events are found more centrally within host galaxies, as also observed by Galbany et al. (2012).

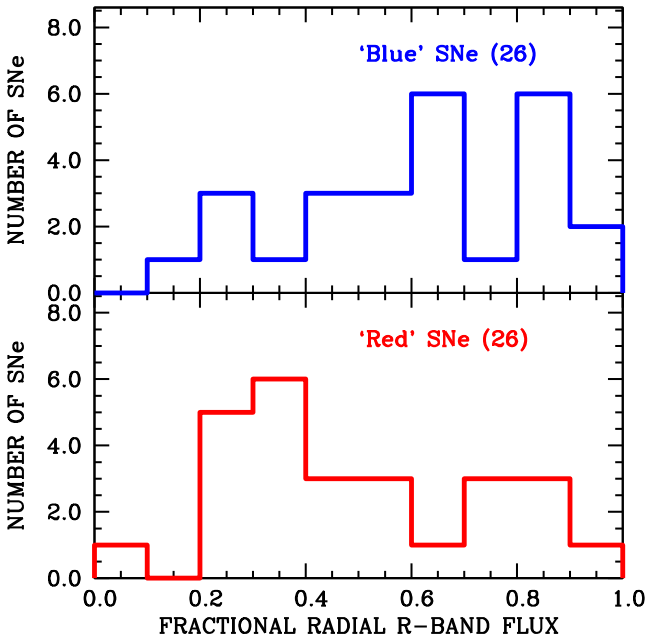

Figure 14. Histogram of fractional radial distribution of the SN Ia population (in star-forming galaxies) with respect to the *R*-band light distribution of their host galaxies, when split by the median $(B-V)_{\rm max}$ of 0.106.

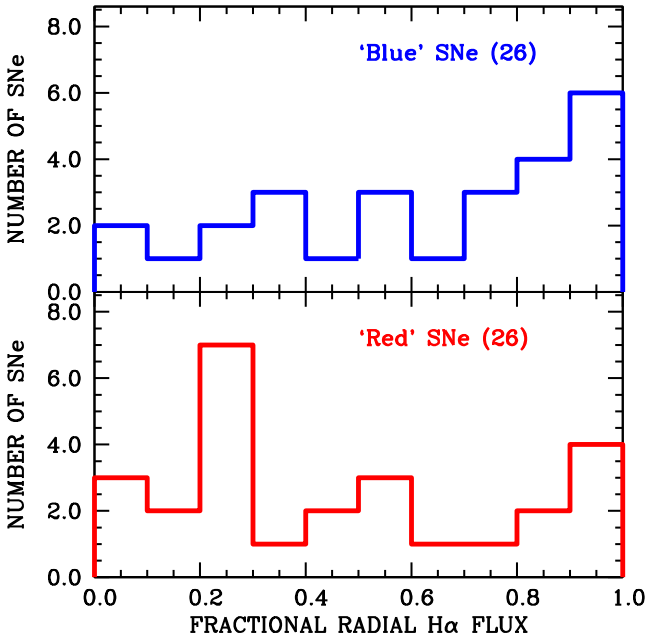

Figure 15. Histogram of fractional radial distribution of the SN Ia population (in star-forming galaxies) with respect to the Hα emission distribution of their host galaxies, when split by the median $(B-V)_{\rm max}$ of 0.106.

4.3 The environments of the 'reddest' SNe Ia

It has been shown that 'redder' SNe are generally found to both fall on regions of more intense SF and in more central parts of galaxies than their 'blue' counterparts. If these results are due to line-of-sight ISM then one may ask if there are SNe which are significantly 'red' but *do not* fall on star-forming regions or in the central parts of their galaxies? We define 'red' SNe as those with a $(B-V)_{\rm max}$ value higher than 0.5. We then compile the data for these SNe in Table 4 where we present SN colours together with their Hα and near-UV NCR values, and their $\rm Fr_R$ and $\rm Fr_{H\alpha}$ values. We find that these 'reddest' SNe indeed generally occur within bright H II regions (as indicated by their NCR values) and in more central regions. The mean Hα NCR value for these 10 SNe is 0.232, higher than the 0.157 for the full sample. In addition, almost 60 per cent of the full sample fall on regions of zero Hα flux, while this falls to 40 per cent for these 10 SNe. In terms of their radial positions, the mean $\rm Fr_R$ for this subset of events is 0.408, compared to 0.554 for the full sample, and the difference is more extreme for $\rm Fr_{H\alpha}$: 0.292 for the subsample, and 0.560 for the full sample. Looking closely at Table 4 there is only one SN where one may argue that the environmental properties cannot explain its 'red' colour: SN 2005ke (the rest of the sample either fall on regions of significant SF or in central regions).[10] We note that this is the 'bluest' SN within this subsample. Below we further discuss the implications of this result.

5 DISCUSSION

In previous sections statistical distributions of SN Ia environments have been presented together with results characterizing the properties of the stellar light found in the vicinity of SNe Ia within star-forming galaxies. Now we further discuss how these results can be understood in terms of progenitor properties and SNe Ia diversity.

5.1 Implications for SN Ia progenitors

It has long been accepted that SNe Ia found within star-forming galaxies have shorter lifetimes than those found within elliptical galaxies, due to the longer lived population of the latter. Indeed, there is now significant evidence in the literature that late-type galaxies host brighter SNe Ia (Hamuy et al. 2000; Sullivan et al. 2006, 2010; Kelly et al. 2010; Lampeitl et al. 2010; D'Andrea et al. 2011; Gupta et al. 2011; Childress et al. 2013; Hayden et al. 2013; Johansson et al. 2013; Pan et al. 2014), and these events are generally assumed to form any 'prompt' progenitor channel. In the current work we have only included star-forming host galaxies within our sample. This is by design, as our main initial goal was to investigate the association of SNe of all types with host galaxy SF. Hence, we remove a large fraction the SN population which is distinct from that found in our sample. However, late-type galaxies have much more diverse stellar populations than those found in ellipticals, and hence one may hope that environmental differences exist that can be used to constrain progenitor properties. These involve the ages traced by different wavebands analysed, together with metallicity gradients within spiral galaxies, and in addition the wide range of line-of-sight extinction found within different regions of star-forming galaxies.

5.1.1 *Constraints on SNe Ia progenitor ages*

SN Ia do not trace the Hα nor the near-UV emission, i.e. the ongoing or recent SF. However, they do seem to trace the *B*-band light extremely well (see Fig. 3). Going further redwards they do not trace the *J*- or *K*-band light. Qualitatively, this suggests that the dominant progenitor population in late-type galaxies is neither extremely prompt nor significantly delayed. We speculate that the population is dominated by progenitors with ages of several hundreds of Myr.

[10] Indeed, other than this SN *all* of the events within this subsample exploded within the central 50 per cent of their host galaxy light.

Table 3. Mean Fr values for each of the eight distributions with respect to both the *R* band and Hα light. In column 1 the distribution name is given, followed by the number of events within that distribution in column 2. Then the mean Fr values are given together with their associated standard deviations and standard errors on the mean. Finally, for each set of distributions (i.e. split by either light-curve stretch or colour) we list the KS test probabilities that the two distributions are drawn from the same parent population, followed by the statistical difference (in terms of σ) between the mean values of each population.

Distribution	No. of SNe	Mean Fr (std dev, std error)	KS test	σ difference
Fr_R high stretch	27	0.562 (0.241, 0.047)	>10 per cent	0.08
Fr_R low stretch	28	0.557 (0.248, 0.048)		
$Fr_{H\alpha}$ high stretch	27	0.498 (0.302, 0.059)	>10 per cent	0.97
$Fr_{H\alpha}$ low stretch	28	0.581 (0.323, 0.061)		
Fr_R red $(B-V)_{max}$	26	0.500 (0.245, 0.041)	0.3 per cent	1.90
Fr_R blue $(B-V)_{max}$	26	0.619 (0.234, 0.047)		
$Fr_{H\alpha}$ red $(B-V)_{max}$	26	0.460 (0.311, 0.063)	>10 per cent	1.90
$Fr_{H\alpha}$ blue $(B-V)_{max}$	26	0.625 (0.308, 0.062)		

Table 4. The environment statistics for the 'reddest' SNe Ia in the sample. Here we show all SNe which have $(B-V)_{max}$ higher than 0.5. In column 1 the SN name is listed, followed by the $(B-V)_{max}$ in column 2. In columns 3 and 4 we present the NCR values derived from Hα and near-UV imaging, respectively. Then the Fr_R and $Fr_{H\alpha}$ values are listed in columns 5 and 6, respectively.

SN	$(B-V)_{max}$	NCR Hα	NCR UV	Fr_R	$Fr_{H\alpha}$
1986G	0.839	0.069	...	...	...
1995E	0.679	0.000	0.345	0.394	0.284
1996ai	1.553	0.615	0.232	0.325	0.292
1999bh	0.872	0.856	...	0.418	0.232
1999cl	1.059	0.152	0.264	...	...
2003cg	1.110	0.557	0.369	0.242	0.142
2005A	0.986	0.000	0.398	0.255	0.136
2005ke	0.653	0.000	0.069	0.861	0.815
2006X	1.196	0.067	0.201	...	...
2007N	0.988	0.000	0.000	0.361	0.282

As our technique is statistical in nature, we cannot rule out extreme young or extreme old progenitors for any given SN. However, our results suggest that the *B*-band light distribution within star-forming galaxies is consistent with the stellar population which traces the peak of the SN Ia DTD. Indeed, it has been argued by Childress et al. (2014) that this where the great majority of SNe Ia will arise from within these galaxies. Hα and near-UV emission trace stellar populations with ages of less than around 10 and 100 Myr, respectively. The fact that the SN Ia population investigated here does not follow the light of either tracer of SF constrains the majority of these progenitors to have delay times significantly longer than these limits. The observation that SNe Ia in star-forming galaxies also do not trace the near-IR light distribution – as traced by *J*- and *K*-band observations – would also appear to constrain the majority of their progenitors to have significantly shorter delay times than traced by these near-IR observations. While the SN population shows some degree of correlation with the *R*-band light, it best follows the *B*-band light. We use the output from the population synthesis models of Pietrinferni et al. (2004) to extract the population age where the peak flux coincides with the central wavelength of *B*-band filter observations (note, other such models give very similar results). We find that a population age of ~750 Myr matches well the wavelength range probed by *B*-band observations (which is demonstrated with a different set of models in fig. 9 of Bruzual & Charlot 2003). Hence, this constrains the peak age of progenitors within our star-forming galaxy sample to fall within a similar range.

Raskin et al. (2009), using similar pixel techniques to those used here (but confined to regions in the immediate vicinity of the SN), compared SN Ia environments to analytical galaxy models, concluding that even the 'prompt' SNe Ia progenitor channel exhibits a delay time of 200–500 Myr, consistent with our more qualitative arguments above. An important point here is that Raskin et al. (2009) also commented that SNe Ia and CC SNe show a similar degree of association with the *g*-band light of their host galaxies. However, while we make no comparison between the two SN types with respect to *g*-band light (or more appropriately, *B*-band as analysed here), in Fig. 2 it is clear that SNe Ia do not follow the near-UV emission while SNe II (and other CC types to a higher degree; see Habergham et al. 2014) show almost a perfect one-to-one relation to the recent SF. Hence, this shows that indeed one can separate the two SN types using multiwavelength pixel statistics analysed for complete galaxies.

While the above argues against a progenitor population dominated by extremely young channels for the overall sample analysed, one may speculate that the 'prompt' channel is only a fraction of our sample. In Section 4.1 we indeed separated the sample by 'stretch', where one would assume that the SNe with larger values (i.e. brighter events) are most likely to form the 'prompt' channel.[11] However, there is no difference in the association of the two SN groups with either on-going or recent SF. Hence, even the majority of the most 'prompt' SNe Ia in star-forming galaxies would appear to be constrained to have progenitors with delay times longer than at least 100 Myr. We note the statistical nature of our analysis does not rule out any particular SN having shorter lifetimes. However, we suggest that the relative rate of any population (if it indeed exists) must be quite small.

5.1.2 Radial distributions of SNe Ia: progenitor age or metallicity constraints?

In Section 4.2 it was shown that the central parts of galaxies are underpopulated by SNe Ia, and that it appears unlikely that this is a

[11] We note that given our sample lacks any elliptical galaxy hosts, it is essentially dominated by moderate-stretch 'prompt' SNe in the traditional classification.

selection effect given that SNe Ibc – which are intrinsically dimmer than SNe Ia – do not show any such deficit. This central deficit of SNe Ia with respect to CC SNe was also previously shown by Wang et al. (1997). In addition, as one goes out to larger galactocentric normalized distances there is a suggestion that per unit SF more SNe Ia are being produced (see Fig. 10). One can attempt to explain these results through both progenitor age and metallicity effects. In this section we explore both these possibilities.

A progenitor metallicity effect may manifest itself, when one considers that metallicity gradients are found within galaxies (central regions having higher abundances than outer regions; see e.g. Henry & Worthey 1999). Thus the above results could be interpreted in that SNe Ia prefer to explode within lower abundance regions of galaxies. Indeed there is some suggestion of such a trend in recent observational and theoretical works. Prieto, Stanek & Beacom (2008) concluded that there is no significant low-metallicity threshold (below which SNe Ia are not produced) by investigating global host metallicities. Li et al. (2011) showed that the SN Ia rate per unit mass has a strong relation to host galaxy mass, with more events being produced per unit mass in lower mass galaxies. Quimby et al. (2012) also found an excess of dwarf hosts (i.e. low metallicity) in a sample produced by the non-targeted search of Robotic Optical Transient Search Experiment IIIb (ROTSE-IIIb). These observational results were then used by Kistler et al. (2013), who argued that lower metallicity progenitors will lead to higher WD masses which then elevates the SN Ia rate in low metallicity environments as a higher fraction of WDs are able to explode as a SN Ia. Indeed, a prediction of Kistler et al. (2013) was that the SN Ia rate should be higher in the outer regions of galaxies, which is suggested by our work. It is important to note at this point the earlier theoretical work which in fact predicted the opposite to the above. Kobayashi et al. (1998) proposed that SD progenitors should show a preference for high metallicity because of a lower metallicity limit for the production of SNe Ia. This is related to the strong wind blown by the accreting WD, which was required for the progenitor to reach the Chandrasekhar mass. If metallicity is too low then the wind is too weak for the progenitor to evolve to explosion (Kobayashi et al. 1998). Observations (including our own) appear to rule out such a distinct metallicity effect. However, additional work is needed to further investigate this issue. One possibility is to measure the metallicity at the exact explosion site of SNe Ia. If SNe Ia indeed prefer higher/lower metallicity then one would expect that their explosion sites would have higher/lower values than average regions throughout their galaxies. Such analyses are now possible with the advent of wide field of view integral field spectrographs. It has also been shown that 'redder' events are found more centrally within galaxies. While we discuss this below in terms of progenitor age, and then line-of-sight extinction effects, it is also possible that this could be explained through a metallicity effect, which would imply that 'redder' SNe arise from higher metallicity progenitors.

Progenitor age could also be the explanation for our radial distribution results. Within star-forming spiral galaxies, in addition to metallicity gradients, one observes significant gradients in population SFHs. This is in the sense that the outer regions have SFHs dominated by younger populations, while more central regions have a much higher fraction of old stars. It has been observed that the SN Ia rate per unit mass is highly dependent on the colour of parent populations (galaxies), with Mannucci et al. (2005) showing that the rate per unit mass is much higher in galaxies with bluer colours. Hence, redder, older, more central stellar populations within galaxies have lower SN Ia rate per unit mass, providing an explanation for the lack of SNe in the central parts of the *R*-band light distribution

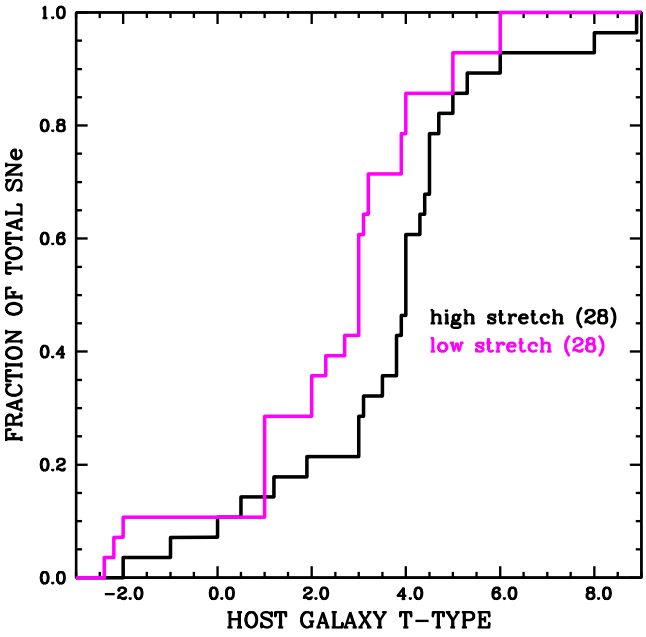

Figure 16. Cumulative plot showing the host galaxy T-type distribution of SNe Ia when divided into high and low stretch samples.

of hosts. Indeed, this argument can also be used to explain that the elevated rate of SN Ia in low-mass galaxies is due to a population age effect (rather than metallicity), as these galaxies are more actively star forming, and hence SN Ia progenitor ages peak at the peak of the DTD, as outlined in Childress et al. (2014). If this second effect of progenitor age is the dominant factor which explains SN Ia environment properties, then one may argue that metallicity plays only a minor role. Indeed, there are now several investigations which argue that progenitor population age is the dominant parameter which correlates with Hubble residuals, and that there is insufficient evidence for any metallicity bias within SN Ia studies.

5.2 A SN Ia sample in exclusively star-forming galaxies

The currently analysed sample is formed exclusively by star-forming galaxies and lacks elliptical hosts. While the SN Ia rate per unit mass is significantly higher in star-forming galaxies (see e.g. Sullivan et al. 2006), ellipticals still produce a significant number of SNe Ia. Distinct SN Ia populations are found in ellipticals and in star-forming galaxies. The population within ellipticals is generally less luminous with lower stretch values. We have found that SN Ia stretch does not appear to correlate with environment *within* host galaxies. Given the classic result of a correlation between SN light-curve morphology with host galaxy type – that higher stretch SNe are found in later morphological types – one may therefore ask how we reconcile this with our result showing no environmental differences stretch separated samples. It could be that our sample is biased in such a way to remove those SNe driving the global stretch trend. To investigate we analyse host galaxy T-types[12] for all SNe with estimated stretch values. In Fig. 16 we show the cumulative distributions of the SN Ia sample with respect to host galaxy type, separated by median stretch. The classic result still holds, in that the high stretch subsample has in general host galaxies of higher T-type. The

[12] Taken from the HyperLeda data base (Makarov et al. 2014): leda.univ-lyon1.fr

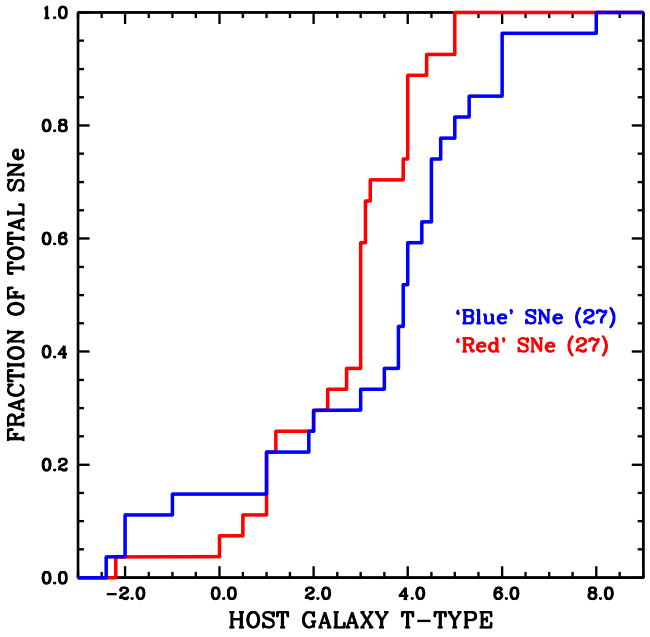

Figure 17. Cumulative plot showing the host galaxy T-type distributions of SNe Ia when divided into 'red' and 'blue' colour samples.

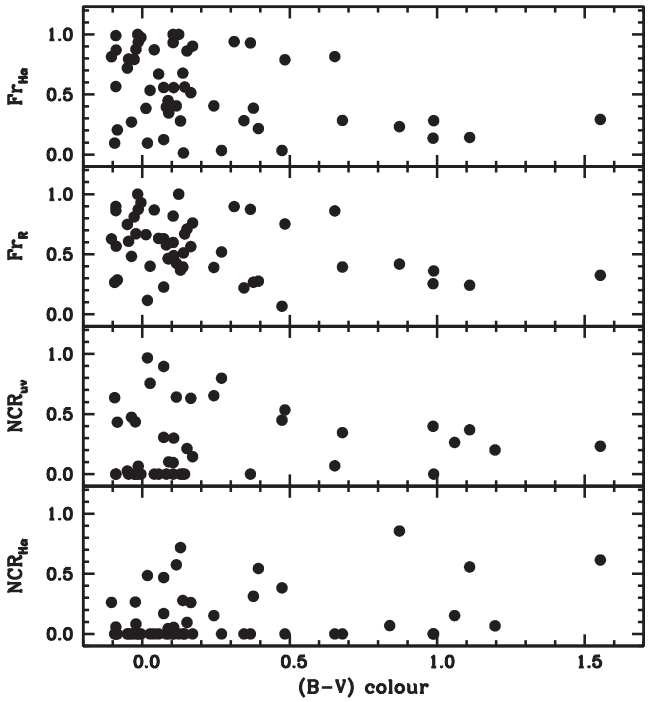

Figure 18. Environmental property indicators against $(B-V)_{\rm max}$.

difference between the two samples is significant at the 2.5 per cent level when a KS test is applied. We also investigate host T-type distributions when the sample is split by the median SN $(B-V)_{\rm max}$ colour, and they are presented in Fig. 17. This shows the possibly surprising result that 'redder' SNe are found in earlier T-type hosts (significant at the ∼5 per cent level). If one assigns the majority of SN Ia colour diversity to ISM effects, then one would expect the opposite result. We note that a similar result was presented by Smith et al. (2012). This is possibly hinting at a metallicity effect, with 'redder' events occurring in higher metallicity (earlier Hubble type) galaxies.

In conclusion, while overall global host galaxy properties (such as age and metallicity) appear to affect the light-curve shape of SNe Ia, the specific stellar populations nearer to the explosion sites of these events do not seem to affect their properties. This is in contrast to CC SNe, where differences between global properties of host galaxies (see e.g. Hakobyan et al. 2014) are in general much smaller than differences of their nearby environments. The main driver of these differing results would appear to be the ages of the respective progenitors. CC SNe have lifetimes of at most several tens of Myr and hence they have little time to move away from their parent stellar populations. On the other hand, SNe Ia most likely have progenitor delay times of at least several 100 Myr, which gives both their progenitors time to move away from their birth sites, but also gives time for the population of stars at their birth sites to evolve significantly. This effectively washes out the information that can be gained on SN Ia progenitors from analysing the stellar populations at the exact explosion sites of SNe Ia.

5.3 SN colour with respect to environmental effects

One of our key findings is that 'redder' SNe are found to occur both nearer to bright H II regions, while at the same time closer to the centres of hosts than their 'bluer' counterparts. Given the results shown in Section 4.3, one may worry that it is the reddest events which are driving these trends, where it is generally accepted that their 'red' colours do indeed arise from ISM extinction. To elucidate this issue we thus cut our sample to only include those SNe with $(B-V)_{\rm max} < 0.2$, which leaves one with a more general sample similar to those usually used for cosmology. Again the sample is split by the median $(B-V)_{\rm max}$. The above findings are completely robust to this further analysis. In this subset of events the 'redder' SNe are generally found to occur close to regions of Hα SF, and at the same time within more central regions.

In Fig. 18 we present SN $(B-V)_{\rm max}$ colours plotted against our four main environment indicators: $\rm NCR_{H\alpha}$, $\rm NCR_{nUV}$, $\rm Fr_{\it R}$, and $\rm Fr_{H\alpha}$. The vast majority of SNe Ia which have Hα NCR values of zero are relatively 'blue' events. There is also a lack of 'blue' SNe with NCR values higher than 0.4: all SNe with negative $(B-V)_{\rm max}$ values have NCR statistics lower than this value, however, for 'redder' events there are many SNe with higher values. With respect to the UV NCR distribution, any trend with SN colour is much less clear, as already shown above. The one obvious observation is that again the majority of events with NCR values of zero are clustered around $(B-V)_{\rm max}$ colours of zero. With respect to the radial values $\rm Fr_{\it R}$ and $\rm Fr_{H\alpha}$, one can see that 'redder' SN in general have much lower radial values. Indeed, SNe with colours 'redder' than 0.7 exclusively have radial values lower than 0.4 (and lower than 0.3 with respect to $\rm Fr_{H\alpha}$). Meanwhile 'bluer' SNe show the full range of radial values, although the very bluest SNe with negative colours appear to have a preference for exploding in the outer regions of their galaxies, as indicated by their large Fr values.

In regions of more intense SF one expects a higher degree of extinction, which is also expected for SNe occurring in more central regions. It is thus probable that the environments where these SNe explode are affecting their colours through line-of-sight ISM extinction effects, i.e. material in the line of sight reddens the light emitted by the SNe through extinction. A key property of SNe spectra which is assumed to trace the presence and amount of material within the line of sight is narrow sodium (NaD) absorption. The strength of this feature is often used to constrain the amount of host galaxy extinction towards SNe (see e.g. discussion in Poznanski, Prochaska & Bloom 2012; Phillips et al. 2013). Hence, within

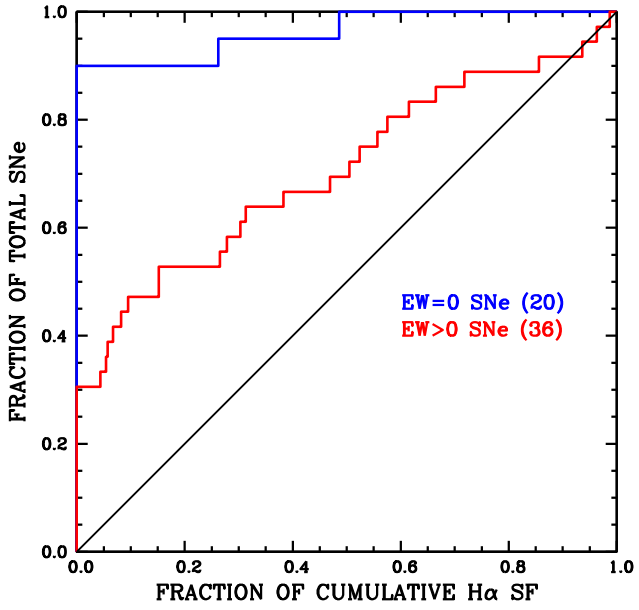

Figure 19. Cumulative Hα NCR plot showing distributions of SNe Ia when split into those SNe with and without NaD absorption in their spectra.

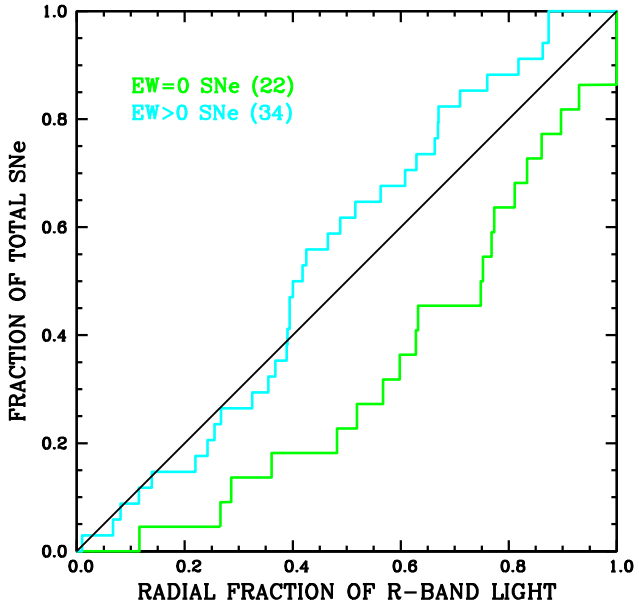

Figure 20. Cumulative plot showing the Fr_R distributions of SNe Ia when the sample is split into those SNe with and without NaD absorption in their spectra.

environments where one expects a higher degree of extinction – closer to H II regions or within more central parts of galaxies – one should also see higher absorption due to line-of-sight material within SNe spectra. The equivalent width (EW) of the unresolved sodium doublet (NaD) was measured for all SNe with available spectra using the method outlined in Förster et al. (2012) and further elaborated in Förster et al. (2013). We then split the samples into those SNe with positive EW measurements, and those without. The results of this analysis are shown in Figs 19 and 20, where we plot the Hα NCR and Fr_R distributions, respectively, for positive and zero EW measurement subsamples. The results are striking. With respect to Hα NCR, we find that the samples are statistically very different with there being less than a 0.1 per cent chance probability of the two EW distributions being drawn from the same parent population. Indeed only 2 of 20 (10 per cent) events with no EW detection fall on regions of positive Hα emission, while this jumps to 24 out of 36 (67 per cent) for SNe with positive EW measurements. Fig. 20 shows that SNe with NaD EW detections are also much more likely to be more central within their galaxies than those without detections, with a $\sim$1 per cent chance of the two distributions being drawn from the same parent population.

The simplest way to explain these results is that ISM material is causing reddening of SNe and also leading to NaD EW detections, where there is more ISM material in the line of sight of SNe when they are found to be coincident with H II regions and/or more centrally. (However, see Pan et al. 2014 who argue that colour diversity is not due to ISM extinction because of the non-correlation with host galaxy extinction as implied from the Balmer decrement.) Circumstellar material in the line of sight could also produce SNe which are both 'redder' and are found to more commonly contain NaD absorption. The presence of such material close to the SN could give clues to the true nature of SN Ia progenitors. This would then imply that environmental properties of explosion sites of SNe Ia are determined by a progenitor property and not simply a chance alignment of a SN with ISM material. A problem with this interpretation is that while it is possible that the radial distribution of SNe Ia could be explained, it is not clear how the circumstellar material (CSM) hypothesis can explain that SNe are more often found within H II regions, given the large offset between the lifetimes of H II regions and those of SN Ia progenitors (where above we have suggested the latter must be more than several 100 Myr). However, there are several observational results which further complicate this matter. It was first observed by Sternberg et al. (2011) that absorption of NaD in SNe Ia spectra shows an excess of blueshifted (with respect to host galaxy velocities) profiles. This was further confirmed by Maguire et al. (2013), who also found that those events showing blueshifted absorption also have stronger absorption components, and were generally found to occur within star-forming galaxies. It is very difficult to explain such blueshifted profiles through ISM properties. In addition, both NaD absorption properties (Förster et al. 2012, 2013) and SN colours (see e.g. Foley, Sanders & Kirshner 2011; Maeda et al. 2011; Foley et al. 2012b) have been shown to correlate with many other SN Ia properties, arguing that at least a fraction of their diversity is intrinsic to the SNe themselves (and not solely from ISM effects). We also note that the centralization of 'red' SNe Ia could hint at a metallicity effect. This would then be consistent with the global host properties of our sample when split by SN colour, as presented in Fig. 17.

Returning to Fig. 19 there is another intriguing observation that has yet to be mentioned. Around 25 per cent of SNe Ia *with* NaD absorption detections fall on regions of *zero Hα flux*. It is possible that this is simply evidence of significant host galaxy extinction outside of bright H II regions. However, an exciting possibility is that these SNe are those where the NaD features are produced by CSM material. Future environment studies correlating the presence of blueshifted NaD absorption with host galaxy SF may be particularly revealing in this context.

It is clear that distinguishing between the effects of ISM and CSM extinction for SNe Ia could have profound implications for the discussion of their progenitors. However, as the above shows, such a differentiation is observationally difficult. We have presented further evidence that line-of-sight material plays a significant role in determining some of the transient features of SNe Ia. Further work will be needed to further elucidate what this means for SN Ia progenitors.

5.4 In the context of previous work

A first study of the immediate environments of SNe Ia was presented by Rigault et al. (2013). These authors measured or set limits on Hα emission at the locations of 89 SNe Ia, where they included elliptical host galaxies. Similar to our work, Rigault et al. showed that moderate stretch SNe were found in all types of Hα environment. With respect to colour they observed that 'redder' SNe were found in higher star-forming environments with a higher flux of Hα emission. This is equivalent to our finding using Hα NCR pixel statistics (see Section 4.1.4 and Fig. 5). Unfortunately we are not in a position to test for environmental effects on Hubble residuals in our sample, as done by those authors, due to the low number of events which could be included in such an analysis. Wang et al. (2013) investigated how spectral velocities of SNe Ia correlate with local environment in terms of radial distributions of SNe (but using normalized distances in place of normalizing to flux as done here) and pixel statistics with respect to *u*-, *g*-, *r*-band light (following the formalism of Fruchter et al. 2006). Similar to our findings, they found that overall the SN Ia population followed the *g* and *r* (somewhat equivalent to the analysis presented with respect to the *B* and *R* light distributions) reasonably well, but not the *u*-band light (see their fig. 3). Wang et al. in particular separated the SN Ia sample into high- and low-velocity events, claiming for two distinct populations given the differences in environment of the two subsamples. High-velocity events were found to be more centrally within hosts and also to explode on brighter regions (although note the lower significance of this trend in a separate sample as shown by Pan et al. 2015). While these results are intriguing, we caution on mixing spiral and elliptical hosts when analysing environments. The stellar populations and their distributions are extremely distinct, and it makes more sense to analyse the two samples separately. Here we do not include such an analysis of environments with respect to spectral velocities within exclusively star-forming host galaxies, but such a study in the future may be revealing to confirm the above claims.

The radial distribution of SNe Ia was found to show a deficit in the central regions of spiral galaxies by van den Bergh (1997), as observed above (also see Wang et al. 1997). Galbany et al. (2012) analysed the radial distribution of a sample $\sim$200 SNe Ia and concluded that SNe in the more central parts of spiral host galaxies SNe Ia have larger colours (or equivalent parameters) than those SNe in the outer regions, similar to what we have shown. A significant difference between our study and those previously is that we normalize radial positions to flux and not distance, meaning we are analysing where within the radial light distribution SNe fall.

Overall the results we present are consistent with those previously presented in the literature. SN stretch does not show any significant correlation with local environment in star-forming galaxies, seen through either measurements of the flux at the exact explosion sites, or through analyses of the radial distributions of stretch subsamples. However, SN colour does seem to show significant correlation with environment.

6 CONCLUSIONS

We have presented statistics on the properties of the environments of SNe Ia within star-forming galaxies. Our main findings are that SNe Ia best trace the *B*-band light distribution within their galaxies, while they do not trace neither the extreme young populations traced by Hα or near-UV emission, nor the evolved populations traced by *J*- and *K*-band light. It is found that 'redder' SNe are more often found both to be coincident with H II regions and are more centrally concentrated within their host galaxies. In addition, SNe with positive NaD EW measurements are also much more likely to be found in central regions and coincident with bright H II regions. Whether this effect is dominated by ISM or CSM material, or some other progenitor property, remains unresolved. We find a central deficit of SNe Ia with respect to the radial distribution of stellar continuum. Finally, the main conclusions to arise from this investigation are listed below.

(i) The SN Ia population best traces the *B*-band light of their host galaxies. This is in contrast to the Hα, near-UV, *J*- and *K*-band light, where the SNe are inconsistent with being drawn from the underlying populations traced by those bands.

(ii) 'Redder' SNe are found to occur closer to H II regions and also more centrally than their 'blue' counterparts. This implies that a significant source of SN colour arises from line-of-sight material producing extinction and hence reddening effects.

(iii) While we recover the host galaxy type stretch relation found by numerous previous authors, we find no evidence that stretch is related to environments *within* host galaxies.

(iv) SNe Ia within star-forming galaxies do not trace the underlying on-going (Hα) or recent (near-UV) SF. This implies that the dominant population of SNe Ia in star-forming galaxies do not originate from progenitors with delay times of less than a few 100 Myr.

(v) Brighter SNe Ia within host galaxies do not follow the spatial distribution of recent SF, implying that even those SNe Ia associated with a relatively young stellar population do not arise from extreme 'prompt' progenitor channels. This effectively rules out progenitor delay times of less than a few 100 Myr for all but a small minority of events

(vi) A deficit of SNe Ia is found within the central 20 per cent of the *R*-band stellar continuum. There is also a suggestion that more SNe Ia per unit SF are produced in the outer regions of galaxies. This observation could be a metallicity effect with lower metallicity populations producing a higher fraction of SNe. Or it could be explained through a progenitor age effect where the central regions of these galaxies have SFHs weighted to older ages, and hence more SNe are produced in the outer regions where younger stellar populations dominate.

ACKNOWLEDGEMENTS

We thank the referee Mike Childress for his positive report, and useful suggestions on improving the manuscript. Mark Sullivan, Gaston Folatelli, Giuliano Pignata, Mark Phillips, Lluis Galbany, Mike Bode, and Stephen Smartt are thanked for useful discussion. We thank the Carnegie Supernova Project for allowing us to use light-curve fits to unpublished photometry of SN 2009ag. MH, FF, and SG-G acknowledge support from the Millennium Institute of Astrophysics (MAS; Programa Iniciativa Científica Milenio del Ministerio de Economía, Fomento y Turismo de Chile, grant IC120009). SG-G thanks CONICYT through FONDECYT grant 3110142. The Liverpool Telescope is operated on the island of La Palma by Liverpool John Moores University in the Spanish Observatorio del Roque de los Muchachos of the Instituto de Astrofisica de Canarias with financial support from the UK Science and Technology Facilities Council. Based on observations made with the Isaac Newton Telescope operated on the island of La Palma by the Isaac Newton Group in the Spanish Observatorio del Roque de los Muchachos of the Instituto de Astrofisica de Canarias, observations made with the 2.2-m MPG/ESO telescope at La Silla, proposal ID:

084.D-0195, and observations made with the Nordic Optical Telescope, operated by the Nordic Optical Telescope Scientific Association at the Observatorio del Roque de los Muchachos, La Palma, Spain, of the Instituto de Astrofisica de Canarias. This research has made use of the NASA/IPAC Extragalactic Database (NED) which is operated by the Jet Propulsion Laboratory, California Institute of Technology, under contract with the National Aeronautics. Some of the data presented in this paper were obtained from the Mikulski Archive for Space Telescopes (MAST). STScI is operated by the Association of Universities for Research in Astronomy, Inc., under NASA contract NAS5-26555. Support for MAST for non-*HST* data is provided by the NASA Office of Space Science via grant NNX13AC07G and by other grants and contracts. We acknowledge the usage of the HyperLeda database (http://leda.univlyon1.fr).

REFERENCES

Altavilla G. et al., 2004, MNRAS, 349, 1344
Anderson J. P., James P. A., 2008, MNRAS, 390, 1527
Anderson J. P., James P. A., 2009, MNRAS, 399, 559
Anderson J. P., Habergham S. M., James P. A., Hamuy M., 2012, MNRAS, 424, 1372
Aubourg É., Tojeiro R., Jimenez R., Heavens A., Strauss M. A., Spergel D. N., 2008, A&A, 492, 631
Baade D. et al., 1999, Messenger, 95, 15
Bartunov O. S., Tsvetkov D. Y., Filimonova I. V., 1994, PASP, 106, 1276
Biscardi I. et al., 2012, A&A, 537, A57
Bloom J. S. et al., 2012, ApJ, 744, L17
Branch D., Miller D. L., 1993, ApJ, 405, L5
Bruzual G., Charlot S., 2003, MNRAS, 344, 1000
Childress M. et al., 2013, ApJ, 770, 108
Childress M. J., Wolf C., Zahid H. J., 2014, MNRAS, 445, 1898
Conley A. et al., 2008, ApJ, 681, 482
Contreras C. et al., 2010, AJ, 139, 519
D'Andrea C. B. et al., 2011, ApJ, 743, 172
Elias-Rosa N. et al., 2006, MNRAS, 369, 1880
Foley R. J., Sanders N. E., Kirshner R. P., 2011, ApJ, 742, 89
Foley R. J. et al., 2012a, ApJ, 744, 38
Foley R. J. et al., 2012b, ApJ, 752, 101
Ford C. H., Herbst W., Richmond M. W., Baker M. L., Filippenko A. V., Treffers R. R., Paik Y., Benson P. J., 1993, AJ, 106, 1101
Förster F., Schawinski K., 2008, MNRAS, 388, L74
Förster F., Wolf C., Podsiadlowski P., Han Z., 2006, MNRAS, 368, 1893
Förster F., González-Gaitán S., Anderson J., Marchi S., Gutiérrez C., Hamuy M., Pignata G., Cartier R., 2012, ApJ, 754, L21
Förster F., González-Gaitán S., Folatelli G., Morrell N., 2013, ApJ, 772, 19
Fruchter A. S. et al., 2006, Nature, 441, 463
Galbany L. et al., 2012, ApJ, 755, 125
Galbany L. et al., 2014, A&A, 572, A38
Gallagher J. S., Garnavich P. M., Caldwell N., Kirshner R. P., Jha S. W., Li W., Ganeshalingam M., Filippenko A. V., 2008, ApJ, 685, 752
Ganeshalingam M. et al., 2010, ApJS, 190, 418
Garnavich P. M. et al., 2004, ApJ, 613, 1120
Gogarten S. M. et al., 2009, ApJ, 691, 115
Gupta R. R. et al., 2011, ApJ, 740, 92
Habergham S. M., Anderson J. P., James P. A., 2010, ApJ, 717, 342
Habergham S. M., James P. A., Anderson J. P., 2012, MNRAS, 424, 2841
Habergham S. M., Anderson J. P., James P. A., Lyman J. D., 2014, MNRAS, 441, 2230
Hachisu I., Kato M., Saio H., Nomoto K., 2012, ApJ, 744, 69
Hakobyan A. A. et al., 2014, MNRAS, 444, 2428
Hamuy M., Phillips M. M., Suntzeff N. B., Schommer R. A., Maza J., Aviles R., 1996a, AJ, 112, 2391
Hamuy M., Phillips M. M., Suntzeff N. B., Schommer R. A., Maza J., Aviles R., 1996b, AJ, 112, 2398
Hamuy M. et al., 1996c, AJ, 112, 2408
Hamuy M., Trager S. C., Pinto P. A., Phillips M. M., Schommer R. A., Ivanov V., Suntzeff N. B., 2000, AJ, 120, 1479
Hayden B. T., Gupta R. R., Garnavich P. M., Mannucci F., Nichol R. C., Sako M., 2013, ApJ, 764, 191
Henry R. B. C., Worthey G., 1999, PASP, 111, 919
Hicken M. et al., 2009, ApJ, 700, 331
Hicken M. et al., 2012, ApJS, 200, 12
Howell D. A. et al., 2009, ApJ, 691, 661
Iben I., Jr, Tutukov A. V., 1984, ApJS, 54, 335
Ivanov V. D., Hamuy M., Pinto P. A., 2000, ApJ, 542, 588
James P. A., Anderson J. P., 2006, A&A, 453, 57
James P. A. et al., 2004, A&A, 414, 23
Jha S. et al., 2006, AJ, 131, 527
Johansson J. et al., 2013, MNRAS, 435, 1680
Kangas T., Mattila S., Kankare E., Kotilainen J. K., Väisänen P., Greimel R., Takalo A., 2013, MNRAS, 436, 3464
Kelly P. L., Kirshner R. P., 2012, ApJ, 759, 107
Kelly P. L., Kirshner R. P., Pahre M., 2008, ApJ, 687, 1201
Kelly P. L., Hicken M., Burke D. L., Mandel K. S., Kirshner R. P., 2010, ApJ, 715, 743
Kelly P. L., Filippenko A. V., Burke D. L., Hicken M., Ganeshalingam M., Zheng W., 2014, preprint (arXiv:1410.0961)
Kennicutt R. C., Jr, 1998, ARA&A, 36, 189
Kistler M. D., Stanek K. Z., Kochanek C. S., Prieto J. L., Thompson T. A., 2013, ApJ, 770, 88
Kobayashi C., Nomoto K., 2009, ApJ, 707, 1466
Kobayashi C., Tsujimoto T., Nomoto K., Hachisu I., Kato M., 1998, ApJ, 503, L155
Krisciunas K., Hastings N. C., Loomis K., McMillan R., Rest A., Riess A. G., Stubbs C., 2000, ApJ, 539, 658
Krisciunas K. et al., 2004, AJ, 128, 3034
Krisciunas K., Prieto J. L., Garnavich P. M., Riley J.-L. G., Rest A., Stubbs C., McMillan R., 2006, AJ, 131, 1639
Lair J. C., Leising M. D., Milne P. A., Williams G. G., 2006, AJ, 132, 2024
Lampeitl H. et al., 2010, ApJ, 722, 566
Leonard D. C., Li W., Filippenko A. V., Foley R. J., Chornock R., 2005, ApJ, 632, 450
Li W., Chornock R., Leaman J., Filippenko A. V., Poznanski D., Wang X., Ganeshalingam M., Mannucci F., 2011, MNRAS, 412, 1473
Lira P. et al., 1998, AJ, 115, 234
Maeda K. et al., 2011, MNRAS, 413, 3075
Maguire K. et al., 2013, MNRAS, 436, 222
Makarov D., Prugniel P., Terekhova N., Courtois H., Vauglin I., 2014, A&A, 570, A13
Mannucci F., Della Valle M., Panagia N., Cappellaro E., Cresci G., Maiolino R., Petrosian A., Turatto M., 2005, A&A, 433, 807
Mannucci F., Della Valle M., Panagia N., 2006, MNRAS, 370, 773
Maoz D., Mannucci F., Li W., Filippenko A. V., Della Valle M., Panagia N., 2011, MNRAS, 412, 1508
Maoz D., Mannucci F., Brandt T. D., 2012, MNRAS, 426, 3282
Maoz D., Mannucci F., Nelemans G., 2014, ARA&A, 52, 107
Maraston C., 2005, MNRAS, 362, 799
Matteucci F., Panagia N., Pipino A., Mannucci F., Recchi S., Della Valle M., 2006, MNRAS, 372, 265
Meikle W. P. S. et al., 1996, MNRAS, 281, 263
Modjaz M. et al., 2008, AJ, 135, 1136
Neill J. D. et al., 2009, ApJ, 707, 1449
Nomoto K., 1982, ApJ, 257, 780
Nugent P. E. et al., 2011, Nature, 480, 344
Pakmor R., Kromer M., Taubenberger S., Sim S. A., Röpke F. K., Hillebrandt W., 2012, ApJ, 747, L10
Pan Y.-C. et al., 2014, MNRAS, 438, 1391
Pan Y.-C., Sullivan M., Maguire K., Gal-Yam A., Hook I. M., Howell D. A., Nugent P. E., Mazzali P. A., 2015, MNRAS, 446, 354
Patat F., Benetti S., Cappellaro E., Danziger I. J., della Valle M., Mazzali P. A., Turatto M., 1996, MNRAS, 278, 111
Perlmutter S. et al., 1997, ApJ, 483, 565

Perlmutter S. et al., 1999, ApJ, 517, 565
Phillips M. M., 1993, ApJ, 413, L105
Phillips M. M. et al., 1987, PASP, 99, 592
Phillips M. M. et al., 2013, ApJ, 779, 38
Pierce M. J., Jacoby G. H., 1995, AJ, 110, 2885
Pietrinferni A., Cassisi S., Salaris M., Castelli F., 2004, ApJ, 612, 168
Pignata G. et al., 2004, MNRAS, 355, 178
Poznanski D., Prochaska J. X., Bloom J. S., 2012, MNRAS, 426, 1465
Prieto J. L., Stanek K. Z., Beacom J. F., 2008, ApJ, 673, 999
Quimby R. M., Yuan F., Akerlof C., Wheeler J. C., Warren M. S., 2012, AJ, 144, 177
Raskin C., Scannapieco E., Rhoads J., Della Valle M., 2009, ApJ, 707, 74
Riess A. G., Press W. H., Kirshner R. P., 1996, ApJ, 473, 88
Riess A. G. et al., 1998, AJ, 116, 1009
Riess A. G. et al., 1999, AJ, 117, 707
Riess A. G. et al., 2005, ApJ, 627, 579
Rigault M. et al., 2013, A&A, 560, A66
Sandage A., Tammann G. A., 1993, ApJ, 415, 1
Scalzo R. et al., 2014, MNRAS, 440, 1498
Scannapieco E., Bildsten L., 2005, ApJ, 629, L85
Schawinski K., Thomas D., Sarzi M., Maraston C., Kaviraj S., Joo S.-J., Yi S. K., Silk J., 2007, MNRAS, 382, 1415
Smith M. et al., 2012, ApJ, 755, 61
Steele I. A. et al., 2004, in Oschmann J. M., Jr, ed., Proc. SPIE, Vol. 5489, Ground-Based Telescopes. SPIE, Bellingham, p. 679
Sternberg A. et al., 2011, Science, 333, 856
Stritzinger M. D. et al., 2011, AJ, 142, 156
Strolger L.-G. et al., 2004, ApJ, 613, 200
Sullivan M. et al., 2006, ApJ, 648, 868
Sullivan M. et al., 2010, MNRAS, 406, 782
Suntzeff N. B. et al., 1999, AJ, 117, 1175
Tsvetkov D. Y., 2006, Peremennye Zvezdy, 26, 3
Tsvetkov D. Y., Elenin L., 2010, Peremennye Zvezdy, 30, 2
Valentini G. et al., 2003, ApJ, 595, 779
van den Bergh S., 1997, AJ, 113, 197
van den Bergh S., Li W., Filippenko A. V., 2002, PASP, 114, 820
Wang B., Han Z., 2012, New Astron. Rev., 56, 122
Wang L., Höflich P., Wheeler J. C., 1997, ApJ, 483, L29
Wang X. et al., 2009, ApJ, 697, 380
Wang X., Wang L., Filippenko A. V., Zhang T., Zhao X., 2013, Science, 340, 170
Wells L. A. et al., 1994, AJ, 108, 2233
Whelan J., Iben I. J., 1973, ApJ, 186, 1007
Worthey G., 1994, ApJS, 95, 107
Zheng W. et al., 2013, ApJ, 778, L15

APPENDIX A: SN ENVIRONMENT STATISTICS

Table A1. SNe environment statistical analyses values. In column 1 the SN name is listed. This is followed by the NCR values derived from Hα, near-UV, *B*-, *R*-, *J*-, and *K*-band in columns 2–7, respectively. In columns 8 and 9 the Fr_R and $Fr_{H\alpha}$ are listed.

SN	$NCR_{H\alpha}$	NCR_{nUV}	NCR_B	NCR_R	NCR_J	NCR_K	Fr_R	$Fr_{H\alpha}$
1937C	0.555	0.240	···	···	···	···	0.272	0.340
1954B	0.466	0.537	0.629	0.719	0.440	0.000	0.253	0.137
1957A	0.000	0.572	···	0.076	···	···	0.797	0.831
1963I	0.317	0.319	0.792	0.557	0.625	0.808	0.111	0.068
1963J	0.000	···	0.721	0.346	0.466	0.000	0.307	0.126
1968E	0.277	0.599	0.567	0.503	0.485	0.471	0.560	0.577
1968I	0.000	0.000	0.639	0.822	0.769	0.774	0.137	0.063
1969C	0.297	···	···	0.709	···	···	0.300	0.178
1971G	0.030	0.038	···	0.011	0.422	0.000	0.794	0.956
1972H	0.000	0.281	0.498	0.344	0.253	0.016	0.646	0.750
1974G	0.000	0.367	0.000	0.336	0.137	0.032	0.772	0.816
1975A	0.000	0.000	···	···	···	···	0.722	0.672
1979B	0.000	···	0.288	0.725	0.000	0.000	0.784	0.670
1981B	0.000	···	···	0.158	···	···	0.731	0.747
1982B	0.000	0.484	0.560	0.367	0.453	0.278	0.507	0.572
1983U	0.000	···	···	···	···	···	0.365	0.735
1986A	0.249	0.038	0.735	0.682	0.397	0.000	0.433	0.437
1986G	0.069	···	···	···	···	···	···	···
1987D	0.000	0.356	···	0.425	···	···	0.485	0.963
1987O	0.000	0.000	···	···	···	···	0.672	0.755
1989A	0.000	0.238	···	0.160	0.000	0.000	0.674	0.726
1989B	0.544	···	···	0.732	···	···	0.276	0.216
1990N	0.000	0.000	···	0.089	···	···	0.869	0.872
1991ak	0.000	0.652	0.454	0.363	0.301	0.000	0.645	0.655
1991T	0.000	0.000	0.355	0.072	0.126	0.253	0.578	0.395
1992bc	0.000	0.000	···	0.000	···	···	0.898	0.566
1992G	0.343	0.539	0.757	0.761	0.707	0.630	0.335	0.351
1992K	0.395	0.663	···	···	···	···	0.214	0.156
1994ae	0.000	0.026	0.261	0.205	0.000	0.099	0.748	0.720
1994S	0.082	0.000	···	0.278	···	···	0.670	0.876
1995al	0.054	0.300	0.333	0.328	0.330	0.234	0.488	0.557

Table A1 – *continued*

SN	$NCR_{H\alpha}$	NCR_{nUV}	NCR_B	NCR_R	NCR_J	NCR_K	Fr_R	$Fr_{H\alpha}$
1995D	0.000	0.000	0.000	0.000	0.000	0.000	0.930	0.975
1995E	0.000	0.345	0.881	0.862	0.846	0.737	0.394	0.284
1996ai	0.615	0.232	0.810	0.801	0.661	0.661	0.325	0.292
1996Z	0.000	···	···	0.000	···	···	0.768	0.748
1997bp	0.095	0.213	···	0.266	···	···	0.710	0.862
1997bq	0.000	0.096	0.184	0.170	0.000	0.000	0.818	0.932
1997do	0.486	0.967	0.940	0.905	0.749	0.736	0.116	0.095
1997dt	0.524	···	···	0.916	···	···	0.355	0.281
1997Y	0.303	···	0.371	0.810	0.633	0.467	0.139	0.259
1998aq	0.262	···	0.460	0.426	0.313	0.083	0.628	0.814
1998bu	0.000	0.798	···	0.424	···	···	0.519	0.034
1998D	0.000	0.000	0.337	0.178	0.208	0.164	0.608	0.795
1998dh	0.044	···	···	0.339	···	···	0.465	0.449
1998eb	0.000	0.175	···	···	···	···	0.516	0.554
1999aa	0.000	0.473	0.638	0.600	0.398	0.513	0.482	0.270
1999bh	0.856	···	0.599	0.446	0.348	0.450	0.418	0.232
1999bv	0.000	···	···	0.000	···	···	0.834	0.618
1999by	0.000	0.534	···	0.160	···	···	0.752	0.789
1999cl	0.152	0.264	···	···	···	···	···	···
1999cp	0.000	0.000	0.000	0.073	0.000	0.000	0.811	0.791
1999gd	0.000	0.000	0.359	0.346	0.186	0.000	0.874	0.929
2000ce	0.505	···	0.500	0.392	0.000	0.135	0.563	0.507
2000E	0.718	0.000	···	···	···	···	0.368	0.279
2001ay	···	···	···	···	···	···	0.638	0.384
2001bg	0.000	0.145	0.207	0.212	0.000	0.000	0.760	0.902
2001cz	0.000	0.102	···	0.363	···	···	0.461	0.346
2001E	0.265	0.435	0.503	0.477	0.283	0.133	0.663	0.384
2001eg	0.000	0.000	0.225	0.265	0.000	0.606	0.605	0.774
2002au	0.096	0.825	0.481	0.374	0.344	0.000	0.764	0.864
2002bs	0.963	0.988	0.993	0.991	0.956	0.934	0.010	0.009
2002cr	0.000	0.066	0.000	0.052	0.000	0.000	0.874	0.936
2002er	0.278	0.000	···	0.564	0.180	···	0.394	0.678
2002fk	0.000	0.636	···	···	···	···	0.266	0.095
2003cg	0.557	0.369	···	0.693	···	···	0.242	0.142
2003cp	0.000	···	0.606	0.509	0.023	0.000	0.494	0.605
2003du	0.000	0.432	0.670	0.000	0.000	···	0.286	0.205
2004bc	0.987	0.821	···	0.966	···	···	0.389	0.189
2004bd	0.665	0.214	0.865	0.862	0.759	0.769	0.115	0.434
2005A	0.000	0.398	···	0.506	···	···	0.255	0.136
2005am	0.000	0.000	0.330	0.000	0.265	0.255	0.632	0.670
2005bc	0.313	···	0.770	0.751	0.716	0.725	0.267	0.386
2005bo	0.152	0.653	0.387	0.456	0.420	0.376	0.390	0.405
2005cf	0.000	0.000	···	···	···	···	1.000	1.000
2005el	0.000	···	···	0.000	···	···	0.567	0.870
2005F	···	···	···	···	···	···	0.975	1.000
2005G	···	···	···	···	···	···	0.773	0.656
2005ke	0.000	0.069	···	···	···	···	0.861	0.815
2005M	···	···	···	···	···	···	0.897	0.940
2005W	0.000	0.000	···	···	···	···	0.669	0.562
2006ax	0.057	0.000	···	0.057	···	···	0.863	0.990
2006ce	0.000	0.000	···	0.090	···	···	0.850	0.887
2006D	0.000	0.000	···	0.366	···	···	0.598	1.000
2006mq	0.000	···	···	···	···	···	···	···
2006N	0.000	0.756	0.560	0.591	0.451	0.592	0.400	0.534
2006ou	0.000	···	···	0.562	···	···	0.220	0.282
2006X	0.067	0.201	···	···	···	···	···	···
2007af	0.469	0.306	···	0.372	···	···	0.629	0.558
2007bm	0.383	0.449	···	0.910	···	···	0.067	0.034
2007N	0.000	0.000	···	0.429	···	···	0.361	0.282
2007S	0.575	0.641	···	0.526	···	···	0.425	0.405
2007sr	0.000	···	···	···	···	···	1.000	1.000
2008bi	0.936	0.722	···	0.906	···	···	0.081	0.029

Table A1 – *continued*

SN	$NCR_{H\alpha}$	NCR_{nUV}	NCR_B	NCR_R	NCR_J	NCR_K	Fr_R	$Fr_{H\alpha}$
2008fv	0.261	0.631	0.373	0.478	0.318	0.152	0.564	0.515
2009ag	0.000	···	···	···	···	···	1.000	1.000
2009ds	0.169	0.896	0.771	0.767	0.722	0.909	0.227	0.124
2009ig	0.000	···	···	0.480	···	···	0.511	0.013
2010eb	0.000	0.000	···	0.000	···	···	1.000	1.000
2011ao	0.000	0.301	···	0.545	···	···	0.398	0.379
2011B	···	···	···		···	···	0.247	1.000
2011dm	0.000	···	···	···	···	···	1.000	1.000
2011dx	0.000	0.209	···	0.218	···	···	0.755	0.706
2011ek	0.000	0.000	···	0.000	···	···	1.000	1.000

This paper has been typeset from a TEX/LATEX file prepared by the author.